

1 **Sea surface temperature variability in the central-western**
2 **Mediterranean Sea during the last 2700 years: a multi-proxy**
3 **and multi-record approach**

4

5 **M. Cisneros¹, I. Cacho¹, J. Frigola¹, M. Canals¹, P. Masqué^{2,3,4}, B. Martrat⁵, M.**
6 **Casado⁵, J. Grimalt⁵, L. D. Pena¹, G. Margaritelli⁶ and F. Lirer⁶**

7 ¹ GRC Geociències Marines, Departament de Dinàmica de la Terra i de l'Oceà, Facultat
8 de Geologia, Universitat de Barcelona, Barcelona, Spain

9 ² Institut de Ciència i Tecnologia Ambientals & Departament de Física, Universitat
10 Autònoma de Barcelona, Bellaterra, Spain

11 ³ School of Natural Sciences and Centre for Marine Ecosystems Research, Edith Cowan
12 University, Joondalup, Australia

13 ⁴ Oceans Institute and School of Physics, The University of Western Australia, Crawley,
14 Australia

15 ⁵ Institut de Diagnosi Ambiental i Estudis de l'Aigua, Consell Superior d'Investigacions
16 Científiques, Barcelona, Spain

17 ⁶ Istituto per l'Ambiente Marino Costiero (IAMC)–Consiglio Nazionale delle Ricerche,
18 Calata Porta di Massa, Interno Porto di Napoli, 80133, Napoli, Italy

19 Correspondence to: M. Cisneros (mbermejo@ub.edu)

20

21

22

23

24

25

26 **ABSTRACT**

27 This study analyses the evolution of sea surface conditions during the last 2700 years in
28 the central-western Mediterranean Sea based on six records as measured on five short
29 sediment cores from two sites north of Minorca (cores MINMC06 and HER-MC-MR3).
30 Sea Surface Temperatures (SSTs) were obtained from alkenones and *Globigerina*
31 *bulloides*-Mg/Ca ratios combined with $\delta^{18}\text{O}$ measurements to reconstruct changes in the
32 regional Evaporation–Precipitation (E–P) balance. We reviewed the *G. bulloides*
33 Mg/Ca-SST calibration and re-adjusted it based on a set of core top measurements from
34 the western Mediterranean Sea. According to the regional oceanographic data, the
35 estimated Mg/Ca-SSTs are interpreted to reflect spring seasonal conditions mainly
36 related to the April–May primary productivity bloom. In contrast, the Alkenone-SSTs
37 signal likely integrates the averaged annual signal.

38 A combination of chronological tools allowed synchronizing the records in a
39 common age model. Subsequently a single anomaly stack record was constructed for
40 each proxy, thus easing to identify the most significant and robust patterns. The
41 warmest SSTs occurred during the Roman Period (RP), which was followed by a
42 general cooling trend interrupted by several centennial-scale oscillations. This general
43 cooling trend could be controlled by changes in the annual mean insolation. Whereas
44 some particularly warm SST intervals took place during the Medieval Climate Anomaly
45 (MCA) the Little Ice Age (LIA) was markedly unstable with some very cold SST events
46 mostly during its second half. The records of the last centuries suggest that relatively
47 low E–P ratios and cold SSTs dominated during negative North Atlantic Oscillation
48 (NAO) phases, although SST records seem to present a close positive connection with
49 the Atlantic Multidecadal Oscillation index (AMO).

50

51 **1 Introduction**

52 The Mediterranean is regarded as one of the world's highly vulnerable regions with
53 regard to the current global warming situation (Giorgi, 2006). This high sensitivity to
54 climate variability has been evidenced in several studies focussed in past natural
55 changes (Rohling et al., 1998; Cacho et al., 1999a; Moreno et al., 2002; Martrat et al.,
56 2004; Reguera, 2004; Frigola et al., 2007; Combourieu Nebout et al., 2009). Paleo-
57 studies focussed mostly in the rapid climate variability of the last glacial period have
58 presented solid evidences of a tied connection between changes in North Atlantic
59 oceanography and climate over the Western Mediterranean Region (Cacho et al., 1999b,
60 2000, 2001; Moreno et al., 2005; Sierro et al., 2005; Frigola et al., 2008; Fletcher and
61 Sanchez-Goñi, 2008). Nevertheless, climate variability during the Holocene and,
62 particularly during the last millennium, is not so well described in this region, although
63 its understanding is crucial to place the nature of the 20th century trends in the recent
64 climate history (Huang, 2004).

65 Some previous studies have already proposed that Holocene centennial climate
66 variability in the western Mediterranean Sea could be linked to NAO variability (Jalut et
67 al., 1997, 2000; Combourieu Nebout et al., 2002; Goy et al., 2003; Roberts et al., 2012;
68 Fletcher et al., 2012). In particular, nine Holocene episodes of enhanced deep
69 convection in the Gulf of Lion (GoL) and surface cooling conditions were described at
70 the same location than this study (Frigola et al., 2007). These events have also been
71 correlated to intensified upwelling conditions in the Alboran Sea and tentatively
72 described as two-phase scenarios driven by distinctive NAO states (Ausín et al., 2015).
73 A growing number of studies reveal considerable climate fluctuations during the last 2
74 kyr (Abrantes et al., 2005; Holzhauser et al., 2005; Kaufman et al., 2009; Lebreiro et al.,
75 2006; Martín-Puertas et al., 2008; Kobashi et al., 2011; Nieto-Moreno et al., 2011,

76 2013; Moreno et al., 2012; PAGES 2K Consortium, 2013; Esper et al., 2014; McGregor
77 et al., 2015). However, there is not uniformity about the exact time-span of the different
78 defined climatic periods such for example the Medieval Climatic Anomaly (MCA),
79 term coined originally by Stine (1994).

80 The existing Mediterranean climatic records for the last 1 or 2 kyr are mostly
81 based on terrestrial source archives such as tree rings (Touchan et al., 2005, 2007;
82 Griggs et al., 2007; Esper et al., 2007; Büntgen et al., 2011; Morellón et al., 2012),
83 speleothem records (Frisia et al., 2003; Mangini et al., 2005; Fleitmann et al., 2009;
84 Martín-Chivelet et al., 2011; Wassenburg et al., 2013), or lake reconstructions (Pla and
85 Catalan, 2005; Martín-Puertas et al., 2008; Corella et al., 2011; Morellón et al., 2012).
86 All of these archives can be good sensors of temperature and humidity changes but
87 often their proxy records mix these two climate variables. Recent efforts have focussed
88 in integrating these 2 kyr records into regional climatic signals and they reveal a
89 complexity in the regional response but also evidence the scarcity of marine records to
90 have a more complete picture (PAGES, 2009; Lionello, 2012).

91 In reference to marine records, they are often limited by the lack of adequate
92 time resolution and accurate chronology to produce detailed comparison with terrestrial
93 source records, although they have the potential to provide a wider range of temperature
94 sensitive proxies. Currently, few marine-source paleoclimate records are available from
95 the last 2 kyr in the Mediterranean Sea (Schilman et al., 2001; Versteegh et al., 2007;
96 Piva et al., 2008; Taricco et al., 2009, 2015; Incarbona et al., 2010; Fanget et al., 2012;
97 Grauel et al., 2013; Lirer et al., 2013, 2014; Di Bella et al., 2014; Goudeau et al., 2015)
98 and they are even more scarce in the Western Basin. The current disperse data is not
99 enough to admit a potential commune pattern of marine Mediterranean climate
100 variability for these two millennia (Taricco et al., 2009; Nieto-Moreno et al., 2011;

101 Moreno et al., 2012 and the references therein).

102 The aim of this study is to characterise changes in surface water properties from
103 the Minorca margin in the Catalan-Balearic Sea (central-western Mediterranean),
104 contributing to a better understanding of the climate variations in this region during the
105 last 2.7 kyr. Sea Surface Temperature (SST) has been reconstructed by means of two
106 independent proxies, Mg/Ca analyses on the planktonic foraminifera *Globigerina*
107 *bulloides* and alkenone derived SST (Villanueva et al., 1997; Lea et al., 1999; Barker et
108 al., 2005; Conte et al., 2006). The application of *G. bulloides*-Mg/Ca as a
109 paleothermometer in the western Mediterranean Sea is tested through the analysis of a
110 series of core top samples from different locations of the western Mediterranean Sea
111 and the calibration reviewed consistently. Mg/Ca thermometry is applied with $\delta^{18}\text{O}$ in
112 order to evaluate changes in the Evaporation–Precipitation (E–P) balance of the basin
113 ultimately linked to salinity (Lea et al., 1999; Pierre, 1999; Barker et al., 2005). One of
114 the limitations for the study of climate evolution of the last 2 kyr is that often the
115 intensity of the climate oscillations is at the limit of detection of the selected proxies. In
116 order to identify significant climatic patterns within the proxy records, the analysis have
117 been performed in a collection of multicores from the same region, and their proxy
118 records have been stacked. The studied time periods have been defined as follows
119 (years expressed as BCE=Before Common Era and CE=Common Era): Talaiotic Period
120 (TP; ending at 123 BCE); Roman Period (RP; from 123 BCE to 470 CE); Dark Middle
121 Ages (DMA; from 470 until 900CE); Medieval Climate Anomaly (MCA; from 900 to
122 1275CE); Little Ice Age (LIA; from 1275 to 1850 CE) and Industrial Era (IE) as the
123 most recent period. The limits of these periods are not uniform across the Mediterranean
124 (Lionello, 2012) and here, the selected ages have been chosen according to historical
125 events in Minorca Island and also to the classic climatic ones defined in literature (i.e.

126 Nieto-Moreno et al., 2011, 2013; Moreno et al., 2012; Lirer et al., 2013, 2014).

127 **2 Climatic and oceanographic settings**

128 The Mediterranean Sea is a semi-enclosed basin located in a transitional zone between
129 different climate regimes, from the temperate zone at the north, to the subtropical zone
130 at the south. Consequently, the Mediterranean climate is characterized by mild wet
131 winters and warm to hot, dry summers (Lionello et al., 2006). Interannual climate
132 variability is very much controlled by the dipole-like pressure gradient between the
133 Azores (high) and Iceland (low) system known as the North Atlantic Oscillation (NAO)
134 (Hurrell, 1995; Lionello and Sanna, 2005; Mariotti, 2011; Ausín et al., 2015). But the
135 northern part of the Mediterranean region is also linked to other midlatitude
136 teleconnection patterns (Lionello, 2012).

137 The Mediterranean Sea is a concentration basin (Béthoux, 1980; Lacombe et al.,
138 1981) and the excess of evaporation with respect to freshwater input is balanced by
139 water exchange at the Strait of Gibraltar (i.e. Pinardi and Masetti, 2000; Malanotte-
140 Rizzoli et al., 2014). The basinwide circulation pattern is prevalently cyclonic (Millot,
141 1999). Three convection cells promote the Mediterranean deep and intermediate
142 circulation: a basinwide open cell and two separated closed cells, one for the Western
143 Basin and one for the Eastern part. The first one connects the two basins of the
144 Mediterranean Sea through the Sicilia Strait, where water masses interchange occurs at
145 intermediate depths. This cell is associated with the inflow of Atlantic Water (AW) at
146 the Strait of Gibraltar and the outflow of the Levantine Intermediate Water (LIW) that
147 flows below the first (Lionello et al., 2006).

148 In the north-western Mediterranean Sea, the Northern Current (NC) represents
149 the main feature of the surface circulation transporting waters alongshore from the
150 Ligurian Sea to the Alboran Sea (Fig. 1a). North-east of the Balearic Promontory a

151 surface oceanographic front separates Mediterranean waters transported by the NC from
152 the Atlantic waters that recently entered the Mediterranean (Millot, 1999; Pinot et al.,
153 2002; André et al., 2005).

154 Deep convection occurs offshore the GoL due to the action of very intense cold
155 and dry winter winds such as the Tramontana and the Mistral. These winds cause strong
156 evaporation and cooling of surface water thus increasing their density until sinking to
157 greater depths leading to Western Mediterranean Deep Water (WMDW) (MEDOC,
158 1970; Lacombe et al., 1985; Millot, 1999). Dense shelf water cascading (DSWC) in the
159 GoL also contributes to the sink of large volumes of water and sediments into the deep
160 basin (Canals et al., 2006).

161 The north-western Mediterranean is subject to an intense bloom in late winter-
162 spring when the surface layer stabilizes, and sometimes to a less intense bloom in
163 autumn, when the strong summer thermocline is progressively eroded (Estrada et al.,
164 1985; Bosc et al., 2004; D'Ortenzio and Ribera, 2009; Siokou-Frangou et al., 2010).
165 SST in the region evolve accordingly with this bloom seasonality, with minima SST in
166 February, which subsequently increases until maxima summer values during August.
167 Afterwards, a SST drop can be observed on October although with some interannual
168 variability (Pastor, 2012).

169 **3 Material and methods**

170 **3.1 Sediment cores description**

171 The studied sediment cores were recovered from a sediment drift built by the action of
172 the southward branch of the WMDW north of Minorca (Fig. 1). Previous studies carried
173 out at this site already described high sedimentation rates ($> 20 \text{ cm kyr}^{-1}$) (Frigola et al.,
174 2007, 2008; Moreno et al., 2012), which initially suggested a suitable location to carry

175 on a detailed study of the last millennia. The cores were recovered from two different
176 stations at about 50 km north of Minorca Island with a multicore system. Cores
177 MINMC06-1 and MINMC06-2 (henceforth MIN1 and MIN2) (40°29'N, 04°01'E;
178 2391m water depth; 31 and 32.5 cm core length, respectively) were retrieved in 2006
179 during HERMES 3 cruise onboard the R/V Thethys II. In reference to the recovery of
180 cores HER-MC-MR3.1, HER-MC-MR3.2 and HER-MC-MR3.3 (henceforth MR3.1,
181 MR3.2 and MR3.3) (40°29'N, 3°37'E; 2117m water depth; 27, 18 and 27 cm core
182 length, respectively) took place in 2009 during HERMESIONE expedition onboard the
183 R/V Hespérides. The distance between the MIN and the MR3 cores is ~30 km and both
184 stations are located in an intermediate position within the sediment drift, which extends
185 along a water depth range from 2000 to 2700m (Frigola, 2012; Velasco et al., 1996;
186 Mauffret et al., 1979), being MIN cores deeper than the MR3 ones by about ~300m.

187 MIN cores were homogeneously sampled at 0.5 cm resolution in the laboratory
188 while for MR3 cores a different strategy was followed. MR3.1 and MR3.2 were initially
189 subsampled with a PVC tube and splitted in two halves for XRF analyses in the
190 laboratory. Both halves of core MR3.1, MR3.1A and MR3.1B, were used for the
191 present work as replicates of the same core and records for each half are shown
192 separately. All MR3 cores were sampled at 0.5 cm resolution for the upper 15 cm and at
193 1 cm for the rest of the core, with the exception of half MR3.1B that was sampled at
194 0.25 cm resolution. MR3 cores were formed by brown-orange nanofossil and
195 foraminifera silty clay, lightly bioturbated, with the presence of enriched layers in
196 pteropods and gastropods fragments and some dark layers.

197 Additionally, core top samples from seven multicores collected at different
198 locations in the western Mediterranean have also been used for the correction of the
199 Mg/Ca-SST calibration from *G. bulloides* (Table 1; Fig. 1).

200 **3.2 Radiocarbon analyses**

201 Twelve ^{14}C AMS dates were performed on cores MIN1, MIN2 and MR3.3 (Table S1,
202 Suppl. Info.) over 4–22mg samples of planktonic foraminifer *Globigerina inflata*
203 handpicked from the $> 355 \mu\text{m}$ fraction. Ages were calibrated with the standard marine
204 correction of 408 years and the regional average marine reservoir correction (ΔR) for
205 the central-western Mediterranean Sea using Calib 7.0 software (Stuiver and Reimer,
206 1993) and the MARINE13 calibration curve (Reimer et al., 2013).

207 **3.3 Radionuclides ^{210}Pb and ^{137}Cs**

208 The concentrations of the naturally occurring radionuclide ^{210}Pb were determined in
209 cores MIN1, MIN2, MR3.1A and MR3.2 by alpha-spectroscopy following Sanchez-
210 Cabeza et al. (1998). Concentrations of the anthropogenic radionuclide ^{137}Cs in core
211 MIN1 were measured by gamma spectrometry using a high purity intrinsic germanium
212 detector. Gamma measurements were also used to determine the ^{226}Ra concentrations
213 via the gamma emissions of ^{214}Pb , used to calculate the excess ^{210}Pb concentrations.
214 Sediment accumulation rates for the last century were calculated using the CIC
215 (constant initial concentration) and the CF : CS (constant flux : constant sedimentation)
216 models (Appleby and Oldfield, 1992; Krishnaswami et al., 1971), constrained by the
217 ^{137}Cs concentration profile for core MIN1 (Masqué et al., 2003).

218 **3.4 Bulk geochemical analyses**

219 The elemental composition of cores MR3.1B and MR3.2 was obtained with a XRF
220 Core-Scanner Avaatech System (CORELAB, University of Barcelona), which is
221 equipped with an optical variable system that allows determining in an independent way
222 the length (10–0.1mm) and the extent (15–2 mm) of the bundle of beams-X. This allows
223 obtaining qualitative information of the elementary composition of the materials. The

224 core surfaces were scraped cleaned and covered with a 4 μ m thin SPEXCertiPrep
225 Ultralene foil to prevent contamination and minimize desiccation (Richter and van der
226 Gaast, 2006). Sampling was performed every 1 cm and scanning took place directly at
227 the split core surface. Among the several measured elements this study has mainly use
228 the Mn profile in the construction of the age models.

229 **3.5 Planktonic foraminifera analyses**

230 Specimens for the planktonic foraminifera *Globigerina bulloides* for Mg/Ca and
231 $\delta^{18}\text{O}$ measurements were picked together from a very restrictive size range (250-355
232 microns) but then crushed and cleaned separately. In core MR3.1B, picking was often
233 performed in the <355 μ m fraction due to the small amount of material (sampling
234 every 0.25 cm). Additionally, quantitative analysis of planktonic foraminifera
235 assemblages was carried out in core MR3.3 and on the upper part of core MR3.1A by
236 using the fraction size above 125 μ m. The 42 studied samples presented abundant and
237 well-preserved planktonic foraminifera.

238 Samples for trace elements analyses were formed by ~45 specimens of *G.*
239 *bulloides*, crushed under glass slides to open the chambers and carefully cleaned
240 applying a sequence of clay removal, oxidative and weak acid cleaning steps (Pena et
241 al., 2005). Only samples from core MR3.1A were cleaned including also the “reductive
242 step”. Instrumental analyses were performed in an inductively coupled plasma mass
243 spectrometer (ICP-MS) Perkin Elmer in the Scientific and Technological Centers of the
244 University of Barcelona (CCiT-UB). A standard solution with a ratio close to the
245 foraminifera values (3.2 mmol mol⁻¹) was run every four samples in order to correct any
246 drift over the measurement runs for MR3.1 halves. Standard solution used on the rest of
247 analyses was low (1.6 mmol mol⁻¹). The average reproducibility of Mg/Ca ratios, taking

248 into account the known standard solutions concentrations, was 97 and 89% for MIN1
249 and MIN2 cores, and 99 and 97% for MR3.1A, MR3.1B and MR3.3 cores, respectively
250 Procedure blanks were also routinely measured in order to detect any potential
251 contamination problem during the cleaning and dissolution procedure. Mn/Ca and
252 Al/Ca ratios were always measured in order to detect any potential contamination
253 problem associated with the presence of Mn oxydes and aluminosilicates (Barker et al.,
254 2003; Lea et al., 2005; Pena et al., 2005).

255 In order to avoid the overestimation of Mg/Ca-SST by detrital contamination,
256 Mn/Ca values $> 0.5 \text{ mmol mol}^{-1}$ were discarded in core MR3.1B and only those higher
257 than 1 mmol mol^{-1} on MIN1 and MR3.3. With regard to Al/Ca data, those values
258 susceptible of contamination were also removed. After this data cleaning any significant
259 statistical correlation existed between Mg/Ca and Mn/Ca; Al/Ca (r has been always
260 lower than 0.29, $p\text{-value}=0.06$).

261 Mg/Ca ratios were transferred into SST values using the calibration proposed in
262 this study (Sect. 4.1). In the case of the record MR3.1A, cleaned with the reductive
263 procedure, the Mg/Ca ratios were about 23% lower than those measured in core
264 MR3.1B without the reductive step. This ratio lowering is expected from the
265 preferential dissolution of the Mg-enriched calcite during the reductive step (Barker et
266 al., 2003; Pena et al., 2005; Yu et al., 2007). The obtained percentage of Mg/Ca
267 lowering is comparable or higher to those previously estimated for different planktonic
268 foraminifera, although data from *G. bulloides* was not previously reported (Barker et al.,
269 2003). SST-Mg/Ca in core MR3.1A was calculated after the Mg/Ca correction of this
270 23% offset and applying the same calibration than with the other records.

271 Stable isotopes measurements were performed on 10 specimens of *G. bulloides*
272 after sonically cleaned in methanol to remove fine-grained particles. Analyses were

273 performed in a Finnigan-MAT 252 mass spectrometer fitted with a carbonate
274 microsampler Kiel-I in the CCiT-UB. Analytical precision of laboratory standards for
275 $\delta^{18}\text{O}$ is better than 0.08 ‰. Calibration to Vienna Pee Dee Belemnite or V-PDB was
276 carried out by means NBS-19 standards (Coplen, 1996).

277 Seawater $\delta^{18}\text{O}$ ($\delta^{18}\text{O}_{\text{sw}}$) was obtained after removing the temperature effect on
278 the *G. bulloides* $\delta^{18}\text{O}$ record by applying the Mg/Ca-SST records in the Shackleton
279 Paleotemperature Equation (Shackleton, 1974). The results are expressed in the water
280 standard SMOW ($\delta^{18}\text{O}_{\text{sw}}$) after the correction of Craig (1965). It was also considered
281 the use of specific temperature equations for *G. bulloides* (Bemis et al., 1998; Mulitza et
282 al., 2003), but the core tops estimates provided $\delta^{18}\text{O}_{\text{sw}}$ values of 2.1 -1.5 SMOW‰,
283 significantly higher than those (~1.2 SMOW‰) measured in water samples from the
284 central-western Mediterranean Sea (Pierre, 1999). Considering that the core top $\delta^{18}\text{O}_{\text{sw}}$
285 estimates, after the application of the empirical Shackleton (1974) paleotemperature
286 equation, averaged 1.1 SMOW‰ and thus closer to the actual water measurements, it
287 was decided that this equation was providing more realistic oceanographical conditions
288 in this location.

289 **3.6 Alkenones**

290 Measurements of the relative proportion of unsaturated C_{37} alkenones, namely U^{k}_{37}
291 index, were carried out in order to obtain SST records on the studied cores. Detailed
292 information about the methodology and equipment used in C_{37} alkenone determination
293 can be found in Villanueva et al. (1997). The precision of this paleothermometry tool
294 has been determined as close as $\pm 0.5^\circ\text{C}$ (Eglinton et al., 2001). Furthermore, taking
295 into account duplicate alkenone analysis carried out in core MR3.3, the precision
296 achieved results better than $\pm 0.8^\circ\text{C}$. Reconstruction of SST records was based on the

297 global calibration of Conte et al. (2006), which considers a estimation standard error of
298 1.1°C in surface sediments.

299 **4 Sea surface temperatures and $\delta^{18}\text{O}$ data**

300 **4.1 Mg/Ca-SST calibration**

301 The Mg/Ca ratio measured in *G. bulloides* is a widely used proxy to reconstruct SST
302 (Barker et al., 2005) although available calibrations can provide very different results
303 (Lea et al., 1999; Mashiotta et al., 1999; Elderfield and Ganssen, 2000; Anand et al.,
304 2003; McConnell and Thunell, 2005; Cl  roux et al., 2008; Thornalley et al., 2009;
305 Patton et al., 2011). Apparently, the regional Mg/Ca-temperature response varies due to
306 parameters that have not yet been identified (Patton et al., 2011). A further difficulty
307 arises from the questioned Mg/Ca-thermal signal in high salinity regions such as the
308 Mediterranean Sea where anomalous high Mg/Ca values have been observed (Ferguson
309 et al., 2008). This apparent high salinity sensitivity in foraminifera-Mg/Ca ratios is
310 under discussion and it has not been supported by recent culture experiments (H  nisch
311 et al., 2013), which in addition, could be attributed to diagenetic overprints (Hoogakker
312 et al., 2009; van Raden et al., 2011). In order to test the value of the Mg/Ca ratios in *G.*
313 *bulloides* from the western Mediterranean Sea and also review its significance in terms
314 of seasonality and depth habitat, a set of core top samples from different locations of the
315 western Mediterranean Sea have been analysed. Core-top samples were recovered using
316 a multicorer system and they can be considered as representative of near or present
317 conditions (Masqu   et al., 2003; Cacho et al., 2006). The studied cores are included in
318 the 35–45   N latitude range (Table 1 and Fig. 1) and mostly represent two different
319 trophic regimes, defined by the classical spring bloom (the most north-western basin)
320 and an intermittently bloom (D’Ortenzio and Ribera, 2009).

321 The obtained Mg/Ca ratios have been compared with the isotopically derived
322 calcification temperatures based on the $\delta^{18}\text{O}$ measurements performed also in *G.*
323 *bulloides* from the same samples. This estimation was performed after applying the
324 Shackleton (1974) paleotemperature equation and using the $\delta^{18}\text{O}_{\text{water}}$ data published by
325 Pierre (1999), taking always into consideration the values of the closer stations and
326 from the top 100 m. The resulting Mg/Ca-SST data have been plotted together with
327 those *G. bulloides* data points from North Atlantic core tops previously published by
328 Elderfield and Ganssen (2000). The resulting high correlation ($r^2 = 0.92$; Fig. 2a)
329 strongly supports the dominant thermal signal in the Mg/Ca ratios of the central-western
330 Mediterranean Sea. Thus, the new data set from the Mediterranean core tops improves
331 the sample coverage over the warm end of the calibration and the resulting exponential
332 function indicates 9.4 % sensitivity in the Mg uptake respect to temperature, which is in
333 agreement with the described range in the literature (i.e., Elderfield and Ganssen, 2000;
334 Barker et al., 2005; Patton et al., 2011). The new calibration obtained from the
335 combination of Mg/Ca-SST data from the western Mediterranean Sea and Atlantic
336 Ocean is:

$$337 \quad Mg / Ca = 0.7045(\pm 0.0710)e^{0.0939(\pm 0.0066)T} \quad (1)$$

338 The Mg/Ca-SST signal of *G. bulloides* has been compared with a compilation of water
339 temperature profiles of the first 200 m measured between 1945–2000 yr in stations
340 close to the studied core tops (MEDAR GROUP, 2002). Although significant regional
341 and interannual variations have been observed, the obtained calcification temperatures
342 of our core top samples present the best agreement with temperature values of the upper
343 40 m during the spring months (April–May) (Fig. 2b). This water depth is consistent
344 with that found by plankton tows in the Mediterranean (Pujol and Vergnaud-Grazzini,
345 1995) and with results from multiannual sediment traps monitoring in the Alboran Sea

346 and the GoL where maximum percentages were observed just before the beginning of
347 thermal stratifications (see Bárcena et al., 2004; Bosc et al., 2004; Rigual-Hernández et
348 al., 2012). Although the available information about depth and seasonality distribution
349 of *G. bulloides* is relatively fragmented, this species is generally situated in intermediate
350 or even shallow waters (i.e. Bé, 1977; Ganssen and Kroon, 2000; Schiebel et al., 2002;
351 Rogerson et al., 2004; Thornalley et al., 2009). However, *G. bulloides* has been also
352 observed at deeper depths in some western Mediterranean Sea sub basins (Pujol and
353 Vergnaud-Grazzini, 1995). Extended data with enhanced spatial and seasonal coverage
354 are required in order to better characterise production, seasonality, geographic and
355 distribution patterns of live foraminifers as *G. bulloides*. Nevertheless, the obtained core
356 top data set offers a solid evidence about the seasonal character of the recorded
357 temperature signal in the Mg/Ca ratio.

358 **4.2 A regional stack for SST-Mg/Ca records**

359 The obtained Mg/Ca-SST profiles obtained from our sediment records are plotted with
360 the resulting common age model (see Suppl. Info.) in Fig. 3. The average SST values
361 for the last 2700 years ranged from 16.0 ± 0.9 to $17.8 \pm 0.8^\circ\text{C}$ (uncertainties of average
362 values represent 1σ ; uncertainties of absolute values include analytical precision and
363 reproducibility and also those derived from Mg/Ca-SST calibration). All the
364 temperature reconstructions show the warmest sustained period during the RP,
365 approximately between 170 yr BCE to 300 yr CE, except core MIN2, since this record
366 ends at the RP-DA transition. In addition, all the records show a general consistent
367 cooling trend after the RP with several centennial scale oscillations. Maximum Mg/Ca-
368 SST value is observed in core MR3.3 ($19.6 \pm 1.8^\circ\text{C}$) during the MCA (Fig. 3c) and the
369 minimum is recorded in core MIN1 ($14.4 \pm 1.4^\circ\text{C}$) during the LIA (Fig. 3e). The

370 records present high centennial-scale variability. Particularly, during MCA some warm
371 events reached SST slightly higher than the average of maxima SST (i.e.: $19.6 \pm 1.8^\circ\text{C}$ at
372 ~ 1021 yr CE). These events were far shorter in duration compared to RP (Fig. 3). The
373 highest frequency of intense cold events occurred during the LIA and, especially, the
374 last millennium recorded the minima average Mg/Ca-SST ($15.2 \pm 0.8^\circ\text{C}$). Four of the
375 five records show a pronounced minima SST after year 1275 CE when occurred the
376 onset of LIA. In base to the differentiated patterns in Mg/Ca-SST the LIA period has
377 been divided into two subperiods, an early warmer interval (LIAa) and a later colder
378 interval (LIAb) with the boundary located at 1540 yr CE.

379 One of the main difficulties of working with SST reconstructions for the last
380 millennia is that the targeted climatic signal has often a comparable amplitude to the
381 internal noise of the records due to sampling and proxy limitations. In order to minimize
382 this inherent random noise, all the studied records have been combined in a regional
383 Mg/Ca-SST anomaly stack with the aim to detect the most robust climatic structures
384 along the different records and reduce the individual noise. Firstly, each SST record was
385 converted into a SST anomaly record in relation to its average temperature (Fig. 3f).
386 Secondly, in order to obtain a common sampling interval all records were interpolated.
387 Although interpolation was performed at 3 different resolutions, results did not differ
388 substantially (Fig. 3g). Subsequently, we selected the stack that provided the best
389 resolution offered by our age models (20 yr cm^{-1}) since it preserves very well the high
390 frequency variability of the individual records (Fig. 3g).

391 The obtained stack represents in a clearer way the main SST features described
392 earlier and allows to better identifying the most significant features at centennial-time
393 scale. Abrupt cooling events are mainly recorded during the LIA (-0.5 to $-0.7^\circ\text{C } 100 \text{ yr}^{-1}$)
394 ¹⁾ while abrupt warmings (0.9 to $0.6^\circ\text{C } 100 \text{ yr}^{-1}$) are detected during the MCA. Abrupt

395 events of similar magnitude have been also obtained during the transition LIA/IE.
396 When the whole studied period is considered a long term cooling trend of about -1 to -
397 2°C is observed; however if we focus on the last 1800 yr, since the RP maxima, the
398 observed cooling trend was far more intense, of about -3.1 to -3.5°C.

399 Although the general cooling recorded in our records is very close to the internal
400 noise (-0.3 to -0.8°C kyr⁻¹), is quite consistent with the recent 2k global reconstruction
401 published by McGregor et al., (2015) (best estimation of the SST cooling trend, using
402 the average anomaly method 1 for the periods 1-2000 CE: -0.3°C kyr⁻¹ to -0.4°C kyr⁻¹).

403 **4.3 Oxygen isotope records**

404 Oxygen isotopes measured on carbonates shells of *G. bulloides* ($\delta^{18}\text{O}_c$) and their
405 derived $\delta^{18}\text{O}_{\text{SW}}$ after removing the temperature effect with Mg/Ca-SST records (see
406 Sect. 3.5) are shown in Fig. 4. $\delta^{18}\text{O}_c$ and their derived $\delta^{18}\text{O}_{\text{SW}}$ profiles have been
407 respectively stacked following the same procedure for the SST-Mg/Ca stack (see Sect.
408 4.2). In general terms, all the records present a high stable pattern during the whole
409 period with a weak depleting trend, which is almost undetectable in some cases (i.e.
410 core MIN1).

411 Average $\delta^{18}\text{O}_c$ values range from 1.2 to 1.4 VPDB‰ (and, in general, MR3
412 cores show lightly heavier values (~1.4 VPDB‰) than MIN cores (~1.2 VPDB‰).
413 Lightest $\delta^{18}\text{O}_c$ values (ranged from 1.0 to 1.2 VPDB‰) mostly occur during the RP,
414 although some short light excursions can be also observed during the end of the MCA
415 and/or the LIA. Heaviest values (from 1.4 to 1.8 VPDB‰) are mainly associated with
416 short events during the LIA, the MCA and over the TP/RP transition. A significant
417 increase of $\delta^{18}\text{O}_c$ values is observed at the LIA/IE transition, although a sudden drop is
418 recorded at the end of the stack record (after 1867 yr CE), which could result from a

419 differential influence of the records (i.e. MIN1) and/or extreme artefact (Fig. 4g).

420 After removing the temperature effect on the $\delta^{18}\text{O}_c$ record, the remaining $\delta^{18}\text{O}_{\text{SW}}$
421 record mainly reflects changes in E–P balance, thus resulting as an indirect proxy for
422 sea surface salinity. The average $\delta^{18}\text{O}_{\text{SW}}$ values obtained for the studied period ranged
423 from 1.3 to 1.8 SMOW‰. Heaviest $\delta^{18}\text{O}_{\text{SW}}$ values (from 2.4 to 1.9 SMOW‰) are
424 recorded during the RP when the longest warm period is also observed and some values
425 are notable during MCA too. Enhancements of the E–P balance ($\delta^{18}\text{O}_{\text{SW}}$ heavier values)
426 are coincident with higher SST (Fig. 6). Lightest $\delta^{18}\text{O}_{\text{SW}}$ values (from 0.8 to 1.5
427 SMOW‰) are recorded particularly during the onset and the end of the LIA and also
428 during the MCA. A drop in the E–P balance has been obtained approximately from the
429 end of LIA to the most recent years. The most significant changes in our $\delta^{18}\text{O}_{\text{SW}}$
430 (salinity) stack record correspond to increases in the most recent times and around 1200
431 yr CE (MCA) and to the decrease observed at the end of the LIA (Fig. 4).

432 **4.4 Alkenone-SST records**

433 The two alkenone (U^k_{37})-derived SSTs of MIN cores were already published in Moreno
434 et al. (2012), while the records from MR3 cores are new (Fig. 5). The four Alkenone-
435 SST records show a similar general cooling trend during the studied period and they
436 have also been integrated in a SST anomaly stack (Fig. 5e). The whole cooling trend is
437 of about -1.4°C when the whole studied period is considered and about -1.7°C since the
438 SST maximum recorded during the RP. Alk-SST absolute values uncertainties in this
439 section have been estimated to have a mean value of $\pm 1.1^\circ\text{C}$, taking into account the
440 standard error of estimation (see Sect. 3.6).

441 Previous studies have interpreted the Alkenone-SST signal in the western
442 Mediterranean Sea as an annual average (Ternois et al., 1996; Cacho et al., 1999a, b;

443 Martrat et al., 2004). The average Alkenone-SST values for the studied period (last
444 2700 yr) ranged from 17.0 to 17.4°C.

445 The lowest alkenone temperatures (~16.0°C) have been obtained in core MIN2
446 during the LIAa and, the highest (~18.4°C) in core MR3.3 during the MCA. Values
447 near the average of maxima SST (from 17.9 to 18.4°C) are observed more frequently
448 during TP, RP and MCA, while temperatures during the onset of MCA and LIA show
449 many values closer to the average of minima SST (ranged from 16.0 to 16.2°C). The
450 most abrupt coolings are observed during the LIA and some events were also recorded
451 during MCA (-0.8°C 100 yr⁻¹) and in less magnitude at the transition LIA/IE (-0.5°C
452 100 yr⁻¹). The highest warming rates are recorded during the MCA (0.4°C 100 yr⁻¹) and
453 also during RP.

454 **4.5 Mg/Ca vs. Alkenone SST records**

455 In this section, Alk uncertainties have been considered as estimation standard error of
456 1.1°C considered by the calibration used (see Sect. 3.6) and Mg/Ca-SST uncertainties
457 include analytical precision and reproducibility and also standard error derived from
458 calibration. The obtained averages of Mg/Ca and Alk derived SST are similar (16.9 ±
459 1.4°C vs. 17.2 ± 1.1°C), but the temperature range of the Mg/Ca records shows higher
460 amplitude (see Sect. 4.2 and 4.4).

461 The enhanced Mg/Ca-SST variability is also reflected in the short-term
462 oscillations, at centennial time scale, which are better represented in the Mg/Ca record
463 with oscillations over 0.5°C, while in the alkenone record are shorter. This difference in
464 the signal amplitude cannot be attributed to the different habitat depth since alkenones
465 should reflect the surface photic layer (<50 m), while *G. bulloides* has the capability to
466 develop in a wider and deeper environment (Bé, 1977; Pujol and Vergnaud-Grazzini,

467 1995; Ternois et al., 1996; Sicre et al., 1999; Ganssen and Kroon, 2000; Schiebel et al.,
468 2002; Rogerson et al., 2004; Thornalley et al., 2009), where less changes would be
469 expected. This enhanced Mg/Ca-SST variability could be attributed to the highly
470 restricted seasonal character of its signal, which purely reflects SST changes during the
471 spring season. However, the coccolith signal integrates a wider time period from
472 autumn to spring (Rigual-Hernández et al., 2012, 2013) and, consequently, changes
473 associated with specific seasons become more diluted in the resultant averaged signal.

474 The annual mean corresponding to a Balearic site according to the integrate
475 values of the upper 50 m (Ternois et al., 1996; Cacho et al., 1999a) of the GCC-IEO
476 database that covers January 1994–July 200 is $18.7 \pm 1.1^\circ\text{C}$. Our core tops records,
477 which represent the last decades, show SST values closer to the annual mean in the case
478 of Alk-SST than Mg/Ca-SST that recorded slightly lower values.

479 $U^{k'}_{37}$ -SST records in the western Mediterranean Sea have been interpreted to
480 represent mean annual SST (i.e. Cacho et al., 1999a; Martrat et al., 2004) but seasonal
481 variations in alkenone production could play an important role in the $U^{k'}_{37}$ -SST values
482 (Rodrigo-Gámiz et al., 2014). Considering that during the summer months the
483 Mediterranean Sea is a very stratified and oligotrophic sea, it should be expected
484 reduced alkenone production during this season (Ternois et al., 1996; Sicre et al., 1999;
485 Bárcena et al., 2004; Versteegh et al., 2007; Hernández-Almeida et al., 2011). This
486 observation is further supported by the results from sediment traps located in the GoL
487 showing very low coccolith fluxes during the summer months (Rigual-Hernández et al.,
488 2013), while they show higher values during autumn, winter and spring, reaching
489 maximum values at the end of the winter season, during SST minima. In contrast, high
490 fluxes of *G. bulloides* are almost restricted to the upwelling spring signal, when
491 coccolith fluxes have already started to decrease (Rigual-Hernández et al., 2012, 2013).

492 This different growth season can explain the proxy bias in the SST reconstructions, with
493 more diluted SST signal recorded by the alkenones.

494 Both Mg/Ca-SST and $U^{k'}_{37}$ -SST records show a consistent cooling trend during
495 the studied period (2700 yr) of about $-0.5^{\circ}\text{C kyr}^{-1}$ which is consistent with the recent 2k
496 global reconstruction published by McGregor et al., (2015) (see Sect. 4.2). The recorded
497 cooling since the RP maxima (~ 200 yr CE) is more pronounced in the Mg/Ca-SST (-1.7
498 to $-2.0^{\circ}\text{C kyr}^{-1}$) than in the Alkenone record ($-1.1^{\circ}\text{C kyr}^{-1}$). These coolings are larger
499 than those estimated in the global reconstruction (McGregor et al., 2015) for the last
500 1200 yr (average anomaly method 1: $-0.4^{\circ}\text{C kyr}^{-1}$ to $-0.5^{\circ}\text{C kyr}^{-1}$). It should be noted
501 that the global reconstruction includes Alk-SST from MIN cores (data published in
502 Moreno et al., 2012).

503 The detailed comparison of the centennial SST variability recorded by both
504 proxy stacks consistently indicates a puzzling antiphase (Fig. 11b and c). Although the
505 main trends are consistently parallel in both alkenone and Mg/Ca proxies ($r=0.5$; p
506 value=0) as has been noted in other regions, short-term variability appears to have an
507 opposite character. Results obtained by means of Welch's test indicate that the null
508 hypothesis (means are equal) can be discarded at the 5% error level: t_{observed}
509 (12.446) $> t_{\text{critical}}$ (1.971). This unexpected outcome is a firm evidence of the relevance of
510 the seasonal variability in the climate evolution and would indicate that extreme winter
511 coolings were followed by a more rapid and intense spring warmings. Nevertheless,
512 regarding the low amplitude of several of these oscillations, often close to the error of
513 the proxies, this observation needs to be probed with further constraints as a solid regional
514 feature.

515 5 Discussion

516 5.1 Climate patterns during the last 2.7 kyr

517 Changes in SST in the Minorca region have implications in the surface air mass
518 temperature and moisture source regions that would determine air mass trajectories and
519 ultimately precipitation regime in the Western Mediterranean Region (Millán et al.,
520 2005; Labuhn et al., 2015). Observations of recent data have identified SST as a key
521 factor in the development of torrential rain events in the Western Mediterranean Basin
522 (Pastor et al., 2001), being able to act as a source of potential instability of air masses
523 that transit over these waters (Pastor, 2012). In this line, the combination of SST
524 reconstruction with $\delta^{18}\text{O}_{\text{sw}}$ can provide a light to analyse the connection between
525 thermal changes and moisture export from the central-western Mediterranean Sea
526 during the last 2.7 kyr.

527 The older period recorded by our records is the so-call Talaiotic Period (TP),
528 which corresponds to the Ancient Ages as the Greek Period in other geographic areas.
529 Both studied SST proxies are consistent showing a general cooling trend from ~500 yr
530 BCE and reaching minimum values by the end of the period (~120 yr BCE),
531 synchronously with a reduction in the E–P rate occurred (Fig. 6a–c). Very few other
532 records exist from this time period to compare these trends at regional scale.

533 One of the most outstanding features in the two SST-reconstructions,
534 particularly in the Mg/Ca-SST stack is the warm SST that dominated especially during
535 the second half of the RP (150–400 yr CE). The onset of the RP was relatively cold and
536 a ~2°C warming occurred during the first part of this period. This SST evolution from
537 colder to warmer conditions during the RP is consistent with the isotopic record from
538 the Gulf of Taranto (Taricco et al., 2009) and peat reconstructions from north-western

539 Spain (Martínez-Cortizas et al., 1999), and to some extent to SST proxies in the SE
540 Tyrrhenian Sea (Lirer et al., 2014). However none of these records indicate that the RP
541 was the warmest period of the last 2 kyr. Other records from higher latitudes such as
542 Greenland (Dahl-Jensen et al., 1998), North Europe (Esper et al., 2014), North Atlantic
543 Ocean (Bond et al., 2001; Sicre et al., 2008), speleothem records from North Iberia
544 (Martín-Chivelet et al., 2011) and even the multiproxy PAGES 2K reconstruction from
545 Europe, suggest a rather warmer early RP than late RP and, again, none of these records
546 highlights the roman times as the warmest climate period of the last 2 kyr.
547 Consequently, these very warm RP conditions recorded in the Minorca Mg/Ca-SST
548 stack appears to have a very regional character and suggest a rather heterogeneous
549 thermal response along the European continent and surrounding marine regions.

550 According to the $\delta^{18}\text{O}_{\text{sw}}$ -stack the RP seems to be accompanied by an increase
551 in the E–P ratio (Fig. 6a) as also has been observed in some close regions as Alps
552 (Holzhauser et al., 2005; Joerin et al., 2006). But a lake record from Southern Spain
553 indicates relatively high levels when $\delta^{18}\text{O}_{\text{sw}}$ stack indicates the maximum in E–P ratio
554 (Martín-Puertas et al., 2008). This information is not necessarily contradictory, since
555 enhanced E–P balance in the Mediterranean could induce enhanced precipitation in
556 some of the regions, but more detailed geographical information should be required to
557 really evaluate such situation.

558 After the RP, during the whole DMA and until the MCA, Mg/Ca-SST stack
559 shows a cooling of $\sim 1^\circ\text{C}$ (-0.2°C 100 yr^{-1}), which is of 0.3°C in the case of the
560 Alkenone-SST stack; E–P rate is also decreasing. This trend is in contrast with the
561 general warming trend interpreted in speleothem records from the North Iberia (Martín-
562 Chivelet et al., 2011) or the transition towards drier conditions discussed from Alboran
563 recods (Nieto- Moreno et al., 2011). SST proxies from the Tyrrhenian Sea show a

564 cooling trend after the second half of the DMA and the Roman IV cold/dry phase
565 described by Lirer et al. (2014) that can be tentatively correlated with our SST records
566 (Fig. 6). This cooling phase is also documented in $\delta^{18}\text{O}_{G. ruber}$ record of Gulf of Taranto
567 by Grauel et al. (2013). The heterogeneity of the signal in the different proxies and
568 regions reveals the difficulty to characterise the climate variability during these short
569 periods and reinforce the need of better geographical coverage of individual proxies.

570 Frequently, the Medieval Period is described as a very warm period in numerous
571 regions in the Northern Hemisphere (Hughes and Diaz, 1994; Mann et al., 2008;
572 Martín-Chivelet et al., 2011), but an increasing number of studies are questioning the
573 existence of such a “warm” period (i.e. Chen et al., 2013). Minorca SST-stacks also
574 indicate variable temperatures and it does not stand as a particular warm period within
575 the last 2 kyr (Fig. 6). A significant warming event is centred at ~1000 yr CE and a later
576 cooling with minimum values at about 1200 yr CE (Fig. 6). Higher variability is found
577 in Greenland record (Kobashi et al., 2011) while an early warm MCA and posterior
578 cooling is also observed in temperature reconstructions from Central Europe (Büntgen
579 et al., 2011) and also the European multi-proxy 2k stack for PAGES 2K Consortium
580 (2013). But all these proxies agree in indicating overall warmer temperatures during the
581 MCA than during the LIA. At the MCA/LIA transition a progressive cooling and a
582 change in cyclic oscillation before and after the onset of LIA are visible. This transition
583 is considered the last rapid climate change (RCC) of Mayewski et al. (2004).

584 In the context of the Mediterranean Sea, lake, marine and speleothem proxies
585 suggest drier conditions during the MCA than during the LIA (Moreno et al., 2012;
586 Chen et al., 2013; Nieto-Moreno et al., 2013; Wassenburg et al., 2013). Looking to the
587 $\delta^{18}\text{O}_{sw}$ stack, several oscillations are observed during the MCA and LIA but any clear
588 differentiation between the MCA and LIA can be inferred from this proxy, indicating

589 that these reduced precipitation also involved reduced evaporation in the basin without
590 altering the E–P balance recorded by the $\delta^{18}\text{O}_{\text{sw}}$ proxy. The centennial scale variability
591 detected in both the Mg/Ca-SST stack and $\delta^{18}\text{O}_{\text{sw}}$ stack reveal that higher E–P
592 conditions existed during the warmer intervals (Fig. 6a and c).

593 The LIA stands as a period of high thermal variability according to the Mg/Ca-
594 SST stack and, in base to these records, two substages can be differentiated, a first one
595 when SST oscillations were larger and average temperatures warmer (LIAa) and a
596 second one with shorter oscillations and colder average SST (LIAb). We suggest that
597 LIAa interval could be linked to the Wolf and Spörer solar minima and LIAb
598 corresponds to Maunder and Dalton cold events, in agreement with previous
599 observations (i.e. Vallefuoco et al., 2012).

600 Furthermore, the two LIA substages are also present in the Greenland record
601 (Kobashi et al., 2011). The intense cooling drop ($0.8^{\circ}\text{C } 100 \text{ yr}^{-1}$) at the onset of the
602 LIAb is in agreement with the suggested coolings of 0.5 and 1°C in the Northern
603 Hemisphere (i.e. Matthews and Briffa, 2005; Mann et al., 2009). The described two
604 steps within the LIA are clearer in the Mg/Ca-SST stack than in the Alkenone-SST
605 stack; this is also the case of the alkenone records in Alboran Sea (Nieto-Moreno et al.,
606 2011) and it may be consequence of the general reduced SST variability detected by
607 these proxies (see Sect. 4.5).

608 In terms of humidity, the LIA is described as a period of increased runoff
609 according to the Alboran record (Nieto-Moreno et al., 2011). The available lake level
610 reconstruction from South Spain also reveals a progressive increase after the MCA,
611 reaching a maximum during the LIAb (Martín-Puertas et al., 2008). Different records of
612 flood events in the Iberia Peninsula also report a significant increase of extreme events
613 during the LIA (Barriendos et al., 1998; Benito et al., 2003; Moreno et al., 2008). These

614 conditions are consistent with the described enhanced storm activity over the GoL for
615 the LIA (Sabatier et al., 2012). These conditions could account for the enhanced
616 humidity transport towards the Mediterranean Sea that could produce the reduced E–P
617 ratio detected in the $\delta^{18}\text{O}_{\text{sw}}$ particularly for the LIAb (Fig. 6a).

618 The end of the LIA and onset of the IE is marked in the Mg/Ca-SST stack with a
619 warming phase of about 1°C and less pronounced in the Alkenone-SST stack. This
620 initial warm climatic event is also documented in other Mediterranean regions (Taricco
621 et al., 2009; Marullo et al., 2011; Lirer et al., 2014) and Europe (PAGES 2K
622 Consortium, 2013), which is coincident with a Total Solar Irradiance (TSI)
623 enhancement after Dalton Minima. The two Minorca SST stacks show a cooling trend
624 by the end of the record, which does not seem coherent with the instrumental
625 atmospheric records. In Western Mediterranean, warming has been registered in two
626 main phases: from the mid-1920s to 1950s and from the mid-1970s onwards (Lionello
627 et al., 2006). The Minorca stacks do not show such a warming although they do not
628 cover the second period of warming. Nevertheless, according to instrumental data from
629 the upper layer on the Western Mediterranean since the beginning of the XX century, no
630 warming trends were detected before the 1980s (Vargas-Yáñez et al., 2010).

631 **5.2 Climate forcing mechanisms**

632 The general cooling trend observed in both Mg/Ca-SST and Alkenone-SST stacks
633 presents a good correlation with the summer insolation evolution in the North
634 Hemisphere, which actually dominates the annual insolation balance ($r=0.2$ and 0.8 , p
635 $\text{value}\leq 0.007$, respectively) (Fig. 7). This external forcing has already been proposed to
636 control major SST trends for the whole Holocene period in numerous records from
637 Northern Hemisphere (i.e. Wright, 1994; Marchal et al., 2002; Kaufman et al., 2009;
638 Moreno et al., 2012). Also summer insolation seems to have had a significant influence

639 in the decreasing trend obtained in the isotope records during the whole spanned period
640 ($r=0.4$, p value=0) as has been suggested in the study of Ausín et al. (2015), among
641 others. Nevertheless, another forcing needs to account for the centennial-scale
642 variability of the records, as could be the higher volcanism in the last millennium
643 (McGregor et al., 2015) although no significant correlations have been obtained
644 between our records and volcanic reconstructions (Gao et al., 2008).

645 Solar variability has frequently been suggested as a primary driver of the
646 Holocene millennial-scale variability (i.e. Bond et al., 2001). Several oscillations can be
647 observed in the TSI record (Fig. 7a) whose correlation with the Mg/Ca-SST and
648 Alkenone-SST stacks are low, since most of the major drops in TSI does not correspond
649 to SST cold events; although in the case of the Alkenone-SST stack some degree of
650 correlation exists between the two records ($r=0.5$, p value=0). Nevertheless, TSI does
651 not seem to be the primer driver of the centennial scale SST variability in the studied
652 records.

653 Furthermore, one of the major drivers of Mediterranean inter-annual variability
654 in the Mediterranean region is the NAO (Hurrell, 1995; Lionello and Sanna, 2005;
655 Mariotti, 2011). High state of the NAO produces high pressure over the Mediterranean
656 Sea inducing an increment of the E–P balance and reduces sea level over several sectors
657 of the Mediterranean Sea (Tsimplis and Josey, 2001). During these positive NAO
658 periods, winds over the Mediterranean enhance their north direction, overall salinity
659 increases and formation of dense deep water masses is reinforced as the water exchange
660 through the Corsica channel while the arrival of north storm waves decreases (Wallace
661 and Gutzler, 1981; Tsimplis and Baker, 2000; Lionello and Sanna, 2005). The effect of
662 NAO on Mediterranean temperatures is more ambiguous. Changes during the last
663 decades does not show significant variability with NAO (Luterbacher, 2004; Mariotti,

664 2011) although some studies suggest an opposite response between the two basins with
665 cooling responses in some eastern basins and warming in the western during positive
666 NAO conditions (Demirov and Pinardi, 2002; Tsimplis and Rixen, 2002). Although still
667 controversial, some NAO reconstructions on proxy-records start to be available for the
668 studied period (Lehner et al., 2012; Olsen et al., 2012; Trouet et al., 2012; Ortega et al.,
669 2015). The last millennium is the best-resolved period and that allows a direct
670 comparison with our data to evaluate the potential link to NAO.

671 The correlations between our Minorca temperatures stacks with NAO
672 reconstructions (Fig. 7) are relatively low in the case of Mg/Ca-SST ($r=0.3$, p
673 $\text{value} \leq 0.002$) and not significant in the Alkenone stack, indicating that this forcing is
674 probably not the driver of the main trends in the records, although several uncertainties
675 still exist about the long NAO reconstructions (Lehner et al., 2012). Notwithstanding
676 the relatively low correlation between NAO with Mg/Ca-SST, when a detailed analysis
677 is done focussing on the more intense negative NAO phases, those below 0 (Fig. 7),
678 they mostly appear to correlate with cooling phases in the Mg/Ca-stack. The frequency
679 of these negative events is particularly high during the LIA, and mostly during its
680 second phase (LIAb) when the coldest intervals of our SST-stacks occurred.

681 When the last centuries are compared in detail with the last NAO reconstruction
682 based on several different proxy records of annual resolution and tested with some
683 model assimilations (Ortega et al., 2015), the obtained correlations between $\delta^{18}\text{O}_{\text{sw}}$ and
684 NAO are not statistically significant. But Welch's test results indicate that the null
685 hypothesis (difference between means is 0) cannot be discarded for both proxies, given
686 that calculated p-value (0.913) is higher than the significance level alpha (0.05) (t_{observed}
687 $= -0.109 < t_{\text{critical}} = 1.960$). During the last centuries it can be observed a coherent
688 pattern of variability with our $\delta^{18}\text{O}_{\text{sw}}$ reconstruction, with high (low) isotopic values

689 mainly dominating during positive (negative) NAO phases (Fig. 8). This picture is
690 coherent with the described increase in the E–P balance during high NAO phases
691 described for the last decades (Tsimplis and Josey, 2001), which would also contribute
692 to the concentration of the ^{18}O in the Mediterranean waters. The SST stacks also suggest
693 some degree of correlation between warm SST and high NAO values (Fig. 7) but a more
694 coherent picture is observed when the SST-records are compared to the AMO
695 reconstruction: warm SST dominated during high AMO values (Fig. 9). This picture of
696 salinity changes related to NAO and SST to AMO has actually been also described in
697 base to the analysis of last decades data (Mariotti, 2011; Guemas et al., 2014) and
698 confirms the complex but tied response of the Mediterranean to atmospheric and marine
699 changes over the North Atlantic Ocean.

700 The pattern of high $\delta^{18}\text{O}_{\text{SW}}$ when dominant positive NAO conditions occurred
701 should indicate a reduction in the humidity transport over the Mediterranean region as a
702 consequence of the high atmospheric pressure conditions (Tsimplis and Josey, 2001).
703 To test this hypothesis, the $\delta^{18}\text{O}_{\text{SW}}$ stack and the NAO reconstruction is compared to a
704 proxy interpreted to reflect storm intensity over the GoL (Fig. 8), also linked to
705 increased storm activity in the Eastern North Atlantic (Sabatier et al., 2012). Several
706 periods of increased/decreased storm activity in the GoL correlate indeed with low/high
707 values in the $\delta^{18}\text{O}_{\text{SW}}$ supporting that during negative NAO conditions North European
708 storm waves can more frequently arrive into the Mediterranean Sea (Lionello and
709 Sanna, 2005), contributing to the reduction of the E–P balance (Fig. 8). This data
710 comparison would also support that during these enhanced storm periods, cold SST
711 conditions would dominate in the region as has been previously suggested (Sabatier et
712 al., 2012). Nevertheless, not all the NAO oscillations had identical expression in the
713 compared records and it is coherent with recent observations negative NAO phases that

714 present different atmospheric configuration modes and thus impact over the western
715 Mediterranean Sea (Sáez de Cámara et al., in proof, 2015). Regarding the lower part of
716 the record, the maximum SST temperatures and $\delta^{18}\text{O}_{\text{sw}}$ recorded during the RP (100–
717 300 yr CE) may suggest the occurrence of persistent positive NAO conditions, which
718 would also be consistent with a high pressure driven drop in relatively sea level as has
719 been reconstructed in the north-western Mediterranean Sea (Southern France) (-40 ± 10
720 cm) (Morhange et al., 2013).

721 It is interesting to note that during the DMA a pronounced and intense cooling event is
722 recorded in the Mg/Ca-SST stack at about 500 yr CE. Several references document in
723 the scientific literature the occurrence of the so-called dimming of the sun at 536–537 yr
724 CE (Stothers, 1984). This event, in base to ice core records, has been able to be linked a
725 tropical volcanic eruption (Larsen et al., 2008). Tree-ring data reconstructions from
726 Europe and also historical documents indicate the persistence during several years
727 (536–550 yr CE) of what is described as the most severe cooling across the Northern
728 Hemisphere during the last two millennia (Larsen et al., 2008). Despite the limitations
729 derived from the resolution of our records, Mg/Ca-SST stack record may have caught
730 this cooling and that would prove the robustness of our age models.

731 **6 Summary and conclusions**

732 The review of new core top data of *G. bulloides*-Mg/Ca ratios from the central-western
733 Mediterranean Sea together with previous published data support a consistent
734 temperature sensitivity for the Mediterranean samples and allows to refine the
735 previously calibrations. The recorded Mg/Ca-SST signal from *G. bulloides* is
736 interpreted to reflect April–May conditions from the upper 40m layer. In contrast, the
737 Alkenone-SST estimations are interpreted to integrate a more annual averaged signal,

738 although biased toward the winter months since primary productivity during the
739 summer months in the Mediterranean Sea is extremely low. This more averaged signal
740 of the Alkenone-SST records may explain why they present more smoothed oscillations
741 in comparison to the Mg/Ca-SST records.

742 After the careful construction of a common chronology for the studied
743 multicores, in base to several chronological tools, the individual proxy records have
744 been joined in an anomaly-stacked record to allow a better identification of the more
745 solid patterns and structures. Both Mg/Ca-SST and Alkenone stacks show a consistent
746 cooling trend over the studied period and since the Roman Period maxima this cooling
747 is -1.7 to $-2.0^{\circ}\text{C kyr}^{-1}$ in the Mg/Ca record and less pronounced in the alkenones record
748 ($-1.1^{\circ}\text{C kyr}^{-1}$). This cooling trend seems to be consistent with the general lowering in
749 summer insolation. This general cooling trend is punctuated by several SST oscillations
750 at centennial time scale, which represent: maximum SST dominated during most of the
751 Roman Period (RP); a progressive cooling during Dark Middle Ages (DMA);
752 pronounced variability during Medieval Climate Anomaly (MCA) with two intense
753 warming phases reaching warmer SST than during Little Ice Age (LIA); and very
754 unstable and rather cold LIA, with two substages, a first one with larger SST
755 oscillations and warmer average temperatures (LIAa) and a second one with shorter
756 oscillations and colder average SST (LIAb). The described two stages within the LIA
757 are clearer in the Mg/Ca-SST stack than in the Alkenone-SST record. Comparison of
758 Mg/Ca-SST and $\delta^{18}\text{O}_{\text{SW}}$ stacks indicates that warmer intervals have been accompanied
759 by higher Evaporation–Precipitation (E–P) conditions. The E–P balance oscillations
760 over each defined climatic period during the last 2.7 kyr suggest variations in the
761 thermal change and moisture export patterns in the central-western Mediterranean.

762 The comparison of the Minorca SST-stacks with other paleoclimatic records

763 form Europe suggests a rather heterogonous thermal response along the European
764 continent and surrounding marine regions. Comparison of the new Mediterranean
765 records with the reconstructed variations in Total Solar Irradiance (TSI) does not
766 support a clear connection with this climate forcing. Nevertheless, changes in the North
767 Atlantic Oscillation (NAO) and Atlantic Multidecadal Oscillation (AMO) seem to have
768 exerted a more relevant role controlling climate changes in the region. The negative
769 NAO phases appear to correlate mostly with cooling phases in the Mg/Ca-stack,
770 although this connection is complex and apparently clearer during the most intense
771 negative phases. Nevertheless, when the comparison is focussed in the last 1 kyr, when
772 NAO reconstructions are better constrained, a more consistent pattern arises, with cold
773 and particularly fresher $\delta^{18}\text{O}_{\text{SW}}$ values (reduced E–P balance) during negative NAO
774 phases. A picture of enhanced southward transport of European storm tracks during this
775 period would be coherent with the new data and previous reconstructions of storm
776 activity in the GoL. Nevertheless, the SST-stacks seem to present a more tied relation to
777 AMO during the last four centuries (the available period of AMO reconstructions):
778 warm SST dominated during high AMO values. These evidences would support a close
779 connection between Mediterranean and North Atlantic oceanography for the last 2 kyr.

780 *Acknowledgements.* Cores MINMC06 were recovered by HERMES 3 cruise in 2006 on
781 R/V Thethys II and HER-MC-MR3 cores were collected by HERMESIONE expedition
782 on board of R/V Hespérides in 2009. This research has financially been supported by
783 OPERA (CTM2013-48639-C2-1-R). We thank Generalitat de Catalunya Grups de
784 Recerca Consolidats grant 2009 SGR 1305 to GRC Geociències Marines. Project of
785 Strategic Interest NextData PNR 2011-2013 (www.nextdataproyect.it) has also
786 collaborated in the financing. We are grateful to M. Guart (Dept. d'Estratigrafia,
787 Paleontologia i Geociències Marines, Universitat de Barcelona), M. Romero, T. Padró
788 and J. Perona (Serveis Científico-Tècnics, Universitat de Barcelona), J.M. Bruach
789 (Departament de Física, Universitat Autònoma de Barcelona) and B. Hortelano, Y.
790 Gonzalez-Quinteiro and I. Fernández (Institut de Diagnosi Ambiental i Estudis de
791 l'Aigua, CSIC, Barcelona) for their help with the laboratory work, D. Amblàs for his
792 collaboration with the artwork of maps and to Paleoteam for the unconditional support.
793 E. Garcia-Solsona, S. Giralt and M. Blaauw are acknowledged for their help. B. Martrat
794 acknowledges funding from CSIC-Ramon y Cajal post-doctoral program RYC-2013-
795 14073. M. Cisneros benefited from a fellowship of the University of Barcelona. I.
796 Cacho thanks the ICREA-Academia program from the Generalitat de Catalunya.

797 **References**

- 798 Abrantes, F., Lebreiro, S., Rodrigues, T., Gil, I., Bartels-Jónsdóttir, H., Oliveira, P.,
 799 Kissel, C., and Grimalt, J. O.: Shallow-marine sediment cores record climate
 800 variability and earthquake activity off Lisbon (Portugal) for the last 2000 years,
 801 *Quaternary Sci. Rev.*, 24, 2477–2494, doi:10.1016/j.quascirev.2004.04.009, 2005.
- 802 Anand, P., Elderfield, H., and Conte, M. H.: Calibration of Mg/Ca thermometry in
 803 planktonic foraminifera from a sediment trap time series, *Paleoceanography*, 18,
 804 1050, doi:10.1029/2002PA000846, 2003.
- 805 André, G., Garreau, P., Garnier, V., and Fraunié, P.: Modelled variability of the sea
 806 surface circulation in the North-western Mediterranean Sea and in the Gulf of Lions,
 807 *Ocean Dynam.*, 55, 294–308, 2005.
- 808 Appleby, P. G. and Oldfield, F.: *Application of Lead-210 to Sedimentation Studies*,
 809 Clarendon Press, Oxford, Chapt. 21, 731–778, 1992.
- 810 Ausín, B., Flores, J. A., Sierro, F. J., Cacho, I., Hernández-Almeida, I., Martrat, B., and
 811 Grimalt, J. O.: Atmospheric patterns driving Holocene productivity in the Alboran
 812 Sea (Western Mediterranean): a multiproxy approach, *The Holocene*, 25, 1–13,
 813 doi:10.1177/0959683614565952, 2015.
- 814 Bárcena, M. A., Flores, J. A., Sierro, F. J., Pérez-Folgado, M., Fabres, J., Calafat, A.,
 815 and Canals, M.: Planktonic response to main oceanographic changes in the Alboran
 816 Sea (Western Mediterranean) as documented in sediment traps and surface
 817 sediments, *Mar. Micropaleontol.*, 53, 423–445,
 818 doi:10.1016/j.marmicro.2004.09.009, 2004.
- 819 Barker, S., Greaves, M., and Elderfield, H.: A study of cleaning procedures used for
 820 foraminiferal Mg/Ca paleothermometry, *Geochem. Geophys. Geosy.*, 4, 9,
 821 doi:10.1029/2003GC000559, 2003.
- 822 Barker, S., Cacho, I., Benway, H., and Tachikawa, K.: Planktonic foraminiferal Mg/Ca
 823 as a proxy for past oceanic temperatures: a methodological overview and data
 824 compilation for the Last Glacial Maximum, *Quaternary Sci. Rev.*, 24, 821–834,
 825 doi:10.1016/j.quascirev.2004.07.016, 2005.
- 826 Barriendos, M. and Martin-Vide, J.: Secular climatic oscillations as indicated by
 827 catastrophic floods in the spanish mediterranean coastal area (14th–19th centuries),
 828 *Clim. Change*, 38, 473–491, 1998.
- 829 Bé, A. W. H. and Hutson, W. H.: Ecology of planktonic foraminifera and biogeographic
 830 patterns of life and fossil assemblages in the Indian Ocean, *Micropaleontology*, 23,
 831 369–414, 1977.
- 832 Bemis, B. E., Spero, H. J., Bijma, J. and Lea, D. W.: Reevaluation of the oxygen
 833 isotopic composition of planktonic foraminifera: Experimental results and revised
 834 paleotemperature equations, *Paleoceanography*, 13(2), 150–160,
 835 doi:10.1029/98PA00070, 1998.
- 836 Benito, G., Sopena, A., Sánchez-Moya, Y., Machado, M. J., and Pérez-González, A.:
 837 Palaeoflood record of the Tagus River (Central Spain) during the Late Pleistocene
 838 and Holocene, *Quaternary Sci. Rev.*, 22, 1737–1756, doi:10.1016/S0277-
 839 3791(03)00133-1, 2003.
- 840 Béthoux, J. P.: Mean water fluxes across sections in the Mediterranean Sea, evaluated in
 841 the basis of water and salt budgets and of observed salinities, *Oceanol. Acta*, 3, 79–
 842 88, 1980.
- 843 Blaauw, M. and Christen, J. A.: Flexible paleoclimate age-depth models using an
 844 autoregressive gamma process, *Bayesian Anal.*, 6, 457–474, doi:10.1214/11-BA618,
 845 2011.
- 846

- 847 Bond, G., Kromer, B., Beer, J., Muscheler, R., Evans, M. N., Showers, W., Hoffmann,
848 S., Lottibond, R., Hajdas, I., and Bonani, G.: Persistent solar influence on North
849 Atlantic climate during the holocene, *Science*, 294, 2130–2136,
850 doi:10.1126/science.1065680, 2001.
- 851 Bosc, E., Bricaud, A., and Antoine, D.: Seasonal and interannual variability in algal
852 biomass and primary production in the Mediterranean Sea, as derived from 4 years
853 of SeaWiFS observations, *Global Biogeochem. Cy.*, 18, 2003–2034,
854 doi:10.1029/2003GB002034, 2004.
- 855 Boyle, E. A.: Manganese carbonate overgrowths on foraminifera tests, *Geochim.*
856 *Cosmochim. Ac.*, 47, 1815–1819, 1983.
- 857 Budillon F., Lirer F., Iorio M., Macri P., Sagnotti L., Vallefucio M., Ferraro L., Innangi
858 S., Sahabi M., Tonielli R.: Integrated stratigraphic reconstruction for the last 80 kyr
859 in a deep sector of the Sardinia Channel (Western Mediterranean), *Deep Sea Res*
860 *Part II Top Stud. Oceanogr.*, 56, 725–737, 2009.
- 861 Büntgen, U., Tegel, W., Nicolussi, K., McCormick, M., Frank, D., Trouet, V., Kaplan,
862 J. O., Herzig, F., Heussner, K. U., Wanner, H., Luterbacher, J., and Esper, J.: 2500
863 years of European climate variability and human susceptibility, *Science*, 331, 578–
864 82, doi:10.1126/science.1197175, 2011.
- 865 Cacho, I., Pelejero, C., Grimalt, J. O., Calafat, A., and Canals, M.: C37 alkenone
866 measurements of sea surface temperature in the Gulf of Lions (NW Mediterranean),
867 *Org. Geochem.*, 30, 557–566, 1999a.
- 868 Cacho, I., Grimalt, J. O., Pelejero, C., Canals, M., Sierro, F. J., Flores, J. A., and
869 Shackleton, N.: Dansgaard-Oeschger and Heinrich event imprints in Alboran Sea
870 paleotemperatures, *Paleoceanography*, 14, 698–705, 1999b.
- 871 Cacho, I., Grimalt, J. O., Sierro, F. J., Shackleton, N., and Canals, M.: Evidence for
872 enhanced Mediterranean thermohaline circulation during rapid climatic coolings,
873 *Earth Planet. Sc. Lett.*, 183, 417–429, doi:10.1016/S0012-821X(00)00296-X, 2000.
- 874 Cacho, I., Grimalt, J., Canals, M., Sbaiffi, L., Shackleton, N. J., Schönfeld, J., and Zahn,
875 R.: Variability of the western Mediterranean Sea surface temperature during the last
876 25,000 years and its connection with the Northern Hemisphere climatic changes,
877 *Paleoceanography*, 16, 40–52, 2001.
- 878 Cacho, I., Shackleton, N., Elderfield, H., Sierro, F. J. and Grimalt, J. O.: Glacial rapid
879 variability in deep-water temperature and $\delta^{18}\text{O}$ from the Western Mediterranean Sea,
880 *Quat. Sci. Rev.*, 25, 3294–3311, doi:10.1016/j.quascirev.2006.10.004, 2006.
- 881 Calafat, A. M., Casamor, J., Canals, M., and Ny_eler, F.: Distribución y composición
882 elemental de la materia particulada en suspensión en el Mar Catalano-Balear,
883 *Geogaceta*, 20, 370–373, 1996.
- 884 Calvert, S. and Pedersen, T.: Sedimentary geochemistry of manganese: implications for
885 the environment of formation of manganiferous black shales, *Econ. Geol.*, 91, 36–
886 47, 1996.
- 887 Canals, M., Puig, P., Madron, X. D. De, Heussner, S., Palanques, A., and Fabres, J.:
888 Flushing submarine canyons, *Nature*, 444, 354–357, doi:10.1038/nature05271,
889 2006.
- 890 Chen, L., Zonneveld, K. A. F., and Versteegh, G. J. M.: The Holocene Paleoclimate of
891 the Southern Adriatic Sea region during the “Medieval Climate Anomaly” reflected
892 by organic walled dinoflagellate cysts, *The Holocene*, 23, 645–655,
893 doi:10.1177/0959683612467482, 2013.
- 894 Cléroux, C., Cortijo, E., Anand, P., Labeyrie, L., Bassinot, F., Cailion, N., and
895 Duplessy, J. C.: Mg/Ca and Sr/Ca ratios in planktonic foraminifera: proxies for
896 upper water column temperature reconstruction, *Paleoceanography*, 23, PA3214,

897 doi:10.1029/2007PA001505, 2008.

898 Combourieu Nebout, N., Turon, J., Zahn, R., Capotondi, L., Londeix, L., and Pahnke,
899 K.: Enhanced aridity and atmospheric high-pressure stability over the western
900 Mediterranean during the North Atlantic cold events of the past 50 k.y., *Geology*,
901 30, 863–866, 2002.

902 Combourieu Nebout, N., Peyron, O., Dormoy, I., Desprat, S., Beaudouin, C., Kotthoff,
903 U., and Marret, F.: 5 Rapid climatic variability in the west Mediterranean during the
904 last 25 000 years from high resolution pollen data, *Clim. Past*, 5, 503–521,
905 doi:10.5194/cp-5-503-2009, 2009.

906 Conte, M. H., Sicre, M. A., Rühlemann, C., Weber, J. C., Schulte, S., Schulz-Bull, D.,
907 and Blanz, T.: Global temperature calibration of the alkenone unsaturation index
908 ($U^{K'_{37}}$) in surface waters and comparison with surface sediments, *Geochem.*
909 *Geophys. Geosy.*, 7, 2, doi:10.1029/2005GC001054, 2006.

910 Coplen, T.: New guidelines for reporting stable hydrogen, carbon, and oxygen isotope-
911 ratio data, *Geochim. Cosmochim. Ac.*, 60, 3359–3360, 1996.

912 Corella, J. P., Moreno, A., Morellón, M., Rull, V., Giralt, S., Rico, M. T., Pérez-Sanz,
913 A., and Valero-Garcés, B. L.: Climate and human impact on a meromictic lake
914 during the last 6000 years (Montcortés Lake, Central Pyrenees, Spain), *J.*
915 *Palaeolimnol.*, 46, 351–367, 2011.

916 Craig, H.: The measurement of oxygen isotope paleotemperatures, in: *Stable Isotopes in*
917 *Oceanographic Studies and Paleotemperatures*, edited by: Tongiorgi, E., Consiglio
918 Nazionale delle Ricerche, Laboratorio di Geologia Nucleare, Pisa, 1–24, 1965.

919 D'Ortenzio, F. and Ribera d'Alcalà, M.: On the trophic regimes of the Mediterranean
920 Sea: a satellite analysis, *Biogeosciences*, 6, 139–148, doi:10.5194/bg-6-139-2009,
921 2009.

922 Dahl-Jensen, D., Mosegaard, K., Gundestrup, N., Clow, G. D., Johnsen, S. J., Hansen,
923 A. W., and Balling, N.: Past temperatures directly from the Greenland ice sheet,
924 *Science*, 282, 268–271, 1998.

925 Demirov, E. and Pinardi, N.: Simulation of the Mediterranean Sea circulation from
926 1979 to 1993: Part I. The interannual variability, *J. Marine Syst.*, 33–34, 23–50,
927 2002.

928 Di Bella, L., Frezza, V., Bergamin, L., Carboni, M. G., Falese, F., Mortorelli, E.,
929 Tarragoni, C., and Chiocci, F. L.: Foraminiferal record and high-resolution seismic
930 stratigraphy of the Late Holocene succession of the submerged Ombrone River delta
931 (Northern Tyrrhenian Sea, Italy), *Quatern. Int.*, 328–329, 287–300, 2014.

932 Eglinton, T. I., Conte, M. H., Eglinton, G., and Hayes, J. M.: Proceedings of a
933 workshop on alkenone-based paleoceanographic indicators, *Geochem. Geophys.*
934 *Geosy.*, 2, 1, doi:10.1029/2000GC000122, 2001.

935 Elderfield, H. and Ganssen, G.: Past temperature and $\delta^{18}\text{O}$ of surface ocean waters
936 inferred from foraminiferal Mg/Ca ratios, *Nature*, 405, 442–445, 2000.

937 Esper, J., Frank, D. C., Büntgen, U., Verstege, A., Luterbacher, J., and Xoplaki, E.:
938 Long-term drought severity variations in Morocco, *Geophys. Res. Lett.*, 34, L17702,
939 doi:10.1029/2007GL030844, 2007.

940 Esper, J., Duthorn, E., Krusic, P. J., Timonen, M., and Büntgen, U.: Northern European
941 summer temperature variations over the Common Era from integrated tree-ring
942 density records, *J. Quat. Sci.*, 29, 487–494, doi:10.1002/jqs.2726, 2014.

943 Estrada, M., Vives, F., and Alcaraz, M.: Life and productivity in the open sea, in:
944 *Western Mediterranean*, edited by: Margalef, R., Oxford, Pergamon Press, 148–197,
945 1985.

946 Fanget, A. S., Bassetti, M. A., Arnaud, M., Chi_ oleau, J. F., Cossa, D., Goineau,

947 A., Fontanier, C., Buscail, R., Jouet, G., Maillet, G. M., Negri, A., Dennielou, B.,
948 and Berné, S.: Historical evolution and extreme climate events during the last 400
949 years on the Rhone prodelta (NW Mediterranean), *Mar. Geol.*, 346, 375–391,
950 doi:10.1016/j.margeo.2012.02.007, 2013.

951 Ferguson, J. E., Henderson, G. M., Kucera, M., and Rickaby, R. E. M.: Systematic
952 change of foraminiferal Mg/Ca ratios across a strong salinity gradient, *Earth Planet.*
953 *Sci. Lett.*, 265, 153–166, doi:10.1016/j.epsl.2007.10.011, 2008.

954 Fleitmann, D., Cheng, H., Badertscher, S., Edwards, R. L., Mudelsee, M., G. ktürk, O.
955 M., Fankhauser, A., Pickering, R., Raible, C. C., Matter, A., Kramers, J., and
956 Tüysüz, O.: Timing and climatic impact of Greenland interstadials recorded in
957 stalagmites from northern Turkey, *Geophys. Res. Lett.*, 36, L19707,
958 doi:10.1029/2009GL040050, 2009.

959 Fletcher, W. J. and Sánchez Goñi, M. F.: Orbital and sub-orbital-scale climate impacts
960 on vegetation of the western Mediterranean basin over the last 48 000 yr, *Quaternary*
961 *Res.*, 70, 451–464, 2008.

962 Fletcher, W. J., Debret, M., and Sanchez Goñi, M.: Mid-Holocene emergence of a low-
963 frequency millennial oscillation in western Mediterranean climate: implications for
964 past dynamics of the North Atlantic atmospheric westerlies, *The Holocene*, 23, 153–
965 166, doi:10.1177/0959683612460783, 2012.

966 Frigola, J.: Variabilitat climàtica ràpida a la conca occidental del Mediterrani: registre
967 sedimentològic, Ph.D. Thesis, Dept. of Stratigraphy, Paleontology and Marine
968 Geosciences, University of Barcelona, Spain, 2012.

969 Frigola, J., Moreno, A., Cacho, I., Canals, M., Sierro, F. J., Flores, J. A., Grimalt, J. O.,
970 Hodell, D. A., and Curtis, J. H.: Holocene climate variability in the western
971 Mediterranean region from a deepwater sediment record, *Paleoceanography*, 22,
972 PA2209, doi:10.1029/2006PA001307, 2007.

973 Frigola, J., Moreno, A., Cacho, I., Canals, M., Sierro, F. J., Flores, J. A., and Grimalt,
974 J. O.: Evidence of abrupt changes in Western Mediterranean Deep Water circulation
975 during the last 50 kyr: a high-resolution marine record from the Balearic Sea,
976 *Quatern. Int.*, 181, 88–104, doi:10.1016/j.quaint.2007.06.016, 2008.

977 Frisia, S., Borsato, A., Preto, N., and McDermott, F.: Late Holocene annual growth in
978 three Alpine stalagmites records the influence of solar activity and the North
979 Atlantic Oscillation on winter climate, *Earth Planet. Sci. Lett.*, 216, 411–424, 2003.

980 Ganssen, G. M. and Kroon, D.: The isotopic signature of planktonic foraminifera from
981 NE Atlantic surface sediments: implications for the reconstruction of past oceanic
982 conditions, *J. Geol. Soc. London*, 157, 693–699, 2000.

983 Gao, C., Robock, A. and Ammann, C.: Volcanic forcing of climate over the past 1500
984 years: An improved ice core-based index for climate models, *J. Geophys. Res.*, 113,
985 D23111, doi:10.1029/2008JD010239, 2008.

986 Garcia-Orellana, J., Pates, J. M., Masqué, P., Bruach, J. M., and Sanchez-Cabeza, J. A.:
987 Distribution of artificial radionuclides in deep sediments of the Mediterranean Sea,
988 *Sci. Total Environ.*, 407, 887–98, doi:10.1016/j.scitotenv.2008.09.018, 2009.

989 Giorgi, F.: Climate change hot-spots, *Geophys. Res. Lett.*, 33, L08707,
990 doi:10.1029/2006GL025734, 2006.

991 Goudeau, M. L. S., Reichert, G. J., Wit, J. C., de Nooijer, L. J., Grauel, A. L.,
992 Bernasconi, S. M., and de Lange, G. J.: Seasonality variations in the Central
993 Mediterranean during climate change events in the Late Holocene, *Palaeogeogr.*
994 *Palaeoclimatol.*, 418, 304–318, 2015.

995 Goy, J. L., Zazo, C., and Dabrio, C. J.: A beach-ridge progradation complex reflecting
996 periodical sea-level and climate variability during the Holocene (Gulf of Almeria,

- 997 Western Mediterranean), *Geomorphology*, 50, 251–268, 2003.
- 998 Gray, S. T., Graumlich, L. J., Betancourt, J. L., and Pederson, G. T.: A tree-ring based
999 reconstruction of the Atlantic Multidecadal Oscillation since 1567 A. D., *Geophys.*
1000 *Res. Lett.*, 31,12, doi:10.1029/2004GL019932, 2004.
- 1001 Griggs, C., DeGaetano, A., Kuniholm, P., and Newton, M.: A regional high-frequency
1002 reconstruction of May–June precipitation in the north Aegean from oak tree rings,
1003 AD 1089–1989, *Int. J. Climatol.*, 27, 1075–1089, 2007.
- 1004 Grauel, A. L., Goudeau, M. L. S., de Lange, G. J., and Bernasconi, S. M.: Climate of
1005 the past 2500 years in the Gulf of Taranto, central Mediterranean Sea: a high-
1006 resolution climate reconstruction based on $\delta^{18}\text{O}$ and $\delta^{13}\text{C}$ of *Globigerinoides ruber*
1007 (white), *The Holocene*, 23,1440–1446, doi:10.1177/0959683613493937, 2013.
- 1008 Guemas, V., García-Serrano, J., Mariotti, A., Doblas-Reyes, F., and Caron, L. P.:
1009 Prospects for decadal climate prediction in the Mediterranean region, *Q. J. Roy.*
1010 *Meteor. Soc.*, 141, 580–597, doi:10.1002/qj.2379, 2014.
- 1011 Hernández-Almeida, I., Bárcena, M. Á., Flores, J. A., Sierro, F. J., Sánchez-Vidal, A.,
1012 and Calafat, A.: Microplankton response to environmental conditions in the Alboran
1013 Sea (Western Mediterranean): one year sediment trap record, *Mar. Micropaleontol.*,
1014 78, 14–24, doi:10.1016/j.marmicro.2010.09.005, 2011.
- 1015 Holzhauser, H., Magny, M., and Heinz, J.: Glacier and lake-level variations in west-
1016 central Europe over the last 3500 years, *The Holocene*, 15, 789–801, 2005.
- 1017 Hönisch, B., Allen, K. A., Lea, D. W., Spero, H. J., Eggins, S. M., Arbuszewski, J.,
1018 DeMenocal, P., Rosenthal, Y., Russell, A. D., and Elderfield, H.: The influence of
1019 salinity on Mg/Ca in planktic foraminifers – evidence from cultures, core-top
1020 sediments and complementary $\delta^{18}\text{O}$, *Geochim. Cosmochim. Ac.*,121, 196–213,
1021 2013.
- 1022 Hoogakker, B. A. A., Klinkhammer, G. P., Elderfield, H., Rohling, E. J., and Hayward,
1023 C.: Mg/Ca paleothermometry in high salinity environments, *Earth Planet. Sc. Lett.*,
1024 284, 583–589, doi:10.1016/j.epsl.2009.05.027, 2009.
- 1025 Huang, S.: Merging information from different resources for new insights into climate
1026 change in the past and future, *Geophys. Res. Lett.*, 31, 1–4,
1027 doi:10.1029/2004GL019781, 2004.
- 1028 Hughes, M. K. and Diaz, H. F.: Was there a “Medieval warm period”, and if so, where
1029 and when?, *Clim. Change*, 109–142, 1994.
- 1030 Hurrell, J. W.: Decadal Trends in the North Atlantic Oscillation: regional temperatures
1031 and precipitation, *Science*, 269, 676–679, doi:10.1126/science.269.5224.676, 1995.
- 1032 Incarbona, A., Ziveri, P., Di Stefano, E., Lirer, F., Mortyn, G., Patti, B., Pelosi, N.,
1033 Sprovieri, M., Tranchida, G., Vallefucio, M., Albertazzi, S., Bellucci, L. G.,
1034 Bonanno, A., Bonomo, S., Censi, P., Ferraro, L., Giuliani, S., Mazzola, S., and
1035 Sprovieri, R.: The Impact of the Little Ice Age on Coccolithophores in the Central
1036 Mediterranean Sea, *Clim. Past*, 6, 795–805, doi:10.5194/cp-6-795-2010, 2010.
- 1037 Jalut, G., Esteban Amat, A., Mora, S. R., Fontugne, M., Mook, R., Bonnet, L., and
1038 Gauquelin, T.: Holocene climatic changes in the western Mediterranean: installation
1039 of the Mediterranean climate, *CR. Acad. Sci. Ser. II*, 325, 327–334, 1997.
- 1040 Jalut, G., Esteban Amat, A., Bonnet, L., Gauquelin, T., and Fontugne, M.: Holocene
1041 climatic changes in the Western Mediterranean, from south-east France to south-east
1042 Spain, *Palaeogeogr. Palaeoclimatol.*, 160, 255–290, 2000.
- 1043 Joerin, U. E., Stocker, T. F., Schlu, C., and Physics, E.: Multicentury glacier
1044 fluctuations in the Swiss Alps during the Holocene, *The Holocene*, 16, 697–704,
1045 2006.
- 1046 Kaufman, D. S., Schneider, D. P., McKay, N. P., Ammann, C. M., Bradley, R. S., Bri_

- 1047 a, K. R., Miller, G. H., Otto-Bliesner, B. L., Overpeck, J. P., and Vinther, B. M.:
1048 Recent warming reverses long-term arctic cooling, *Science*, 325, 1236–1239,
1049 doi:10.1126/science.1173983, 2009.
- 1050 Kobashi, T., Kawamura, K., Severinghaus, J. P., Barnola, J. M., Nakaegawa, T.,
1051 Vinther, B. M., Johnsen, S. J., and Box, J. E.: High variability of Greenland surface
1052 temperature over the past 4000 years estimated from trapped air in an ice core,
1053 *Geophys. Res. Lett.*, 38, 21, doi:10.1029/2011GL049444, 2011.
- 1054 Krishnaswami, S., Lal, D., Martin, J. M., and Meybeck, M.: Geochronology of lake
1055 sediments, *Earth. Planet. Sci. Lett.*, 11, 407–414, 1971.
- 1056 Labuhn, I., Genty, D., Vonhof, H., Bourdin, C., Blamart, D., Douville, E., Ruan, J.,
1057 Cheng, H., Edwards, R. L., Pons-Branchu, E., and Pierre, M.: A high-resolution
1058 fluid inclusion $\delta^{18}\text{O}$ record from a stalagmite in SW France: modern calibration and
1059 comparison with multiple proxies, *Quaternary Sci. Rev.*, 110, 152–165,
1060 doi:10.1016/j.quascirev.2014.12.021, 2015.
- 1061 Lacombe, H., Gascard, J. C., Cornella, J., and Béthoux, J. P.: Response of the
1062 Mediterranean to the water and energy fluxes across its surface, on seasonal and
1063 interannual scales, *Oceanol. Acta*, 4, 247–255, 1981.
- 1064 Lacombe, H., Tchernia, P., and Gamberoni, L.: Variable bottom water in the Western
1065 Mediterranean basin, *Prog. Oceanogr.*, 14, 319–338, 1985.
- 1066 Larsen, L. B., Vinther, B. M., Bri_a, K. R., Melvin, T. M., Clausen, H. B., Jones, P. D.,
1067 Siggaard-Andersen, M. L., Hammer, C. U., Eronen, M., Grudd, H., Gunnarson, B.
1068 E., Hantemirov, R. M., Naurzbaev, M. M., and Nicolussi, K.: New ice core evidence
1069 for a volcanic cause of the A.D. 536 dust veil, *Geophys. Res. Lett.*, 35, 1–5,
1070 doi:10.1029/2007GL032450, 2008.
- 1071 Laskar, J., Robutel, P., Joutel, F., Gastineau, M., Correia, A. C. M., and Levrard, B.: A
1072 longterm numerical solution for the insolation quantities of the Earth, *Astron.*
1073 *Astrophys.*, 285, 261–285, 2004.
- 1074 Lea, D. W., Mashiotta, T. A., and Spero, H. J.: Controls on magnesium and strontium
1075 uptake in planktonic foraminifera determined by live culturing, *Geochim.*
1076 *Cosmochim. Ac.*, 63, 2369–2379, 1999.
- 1077 Lea, D. W., Pak, D. K., and Paradis, G.: Influence of volcanic shards on foraminiferal
1078 Mg/Ca in a core from the Galápagos region, *Geochem. Geophys. Geosy.*, 6, 11,
1079 doi:10.1029/2005GC000970, 2005.
- 1080 Lebreiro, S. M., Francés, G., Abrantes, F. F. G., Diz, P., Bartels-Jónsdóttir, H. B.,
1081 Stroynowski, Z. N., Gil, I. M., Pena, L. D., Rodrigues, T., Jones, P. D., Nombela, M.
1082 A., Alejo, I., Bri_a, K. R., Harris, I., and Grimalt, J. O.: Climate change and coastal
1083 hydrographic response along the Atlantic Iberian margin (Tagus Prodelt and Muros
1084 Ría) during the last two millennia, *The Holocene*, 16, 1003–1015, 2006.
- 1085 Lehner, F., Raible, C. C., and Stocker, T. F.: Testing the robustness of a precipitation
1086 proxy-based North Atlantic Oscillation reconstruction, *Quaternary Sci. Rev.*, 45,
1087 85–94, doi:10.1016/j.quascirev.2012.04.025, 2012.
- 1088 Lionello, P.: *The Climate of the Mediterranean Region: From the Past to the Future*,
1089 Elsevier Science, Burlington, MA, 2012.
- 1090 Lionello, P. and Sanna, A.: Mediterranean wave climate variability and its links with
1091 NAO and Indian Monsoon, *Clim. Dynam.*, 25, 611–623, doi:10.1007/s00382-005-
1092 0025-4, 2005.
- 1093 Lionello, P., Malanott-Rizzoli, R., Boscolo, R., Alpert, P., Artale, V., Li, L.,
1094 Luterbacher, J., May, W., Trigo, R., Tsimplis, M., Ulbrich, U., and Xoplaki, E.: The
1095 Mediterranean climate: An overview of the main characteristics and issues, in:
1096 *Mediterranean Climate Variability (MedClivar)*, Elsevier, Amsterdam, 1–26, 2006.

- 1097 Lirer, F., Sprovieri, M., Ferraro, L., Vallefucoco, M., Capotondi, L., Cascella, A.,
1098 Petrosino, P., Insinga, D. D., Pelosi, N., Tamburrino, S., and Lubritto, C.: Integrated
1099 stratigraphy for the Late Quaternary in the eastern Tyrrhenian Sea, *Quatern. Int.*,
1100 292, 71–85, doi:10.1016/j.quaint.2012.08.2055, 2013.
- 1101 Lirer, F., Sprovieri, M., Vallefucoco, M., Ferraro, L., Pelosi, N., Giordano, L., and
1102 Capotondi, L.: Planktonic foraminifera as bio-indicators for monitoring the climatic
1103 changes that have occurred over the past 2000 years in the southeastern Tyrrhenian
1104 Sea, *Integr. Zool.*, 9, 542–54, doi:10.1111/1749-4877.12083, 2014.
- 1105 Luterbacher, J., Dietrich, D., Xoplaki, E., Grosjean, M., and Wanner, H.: European
1106 seasonal and annual temperature variability, trends, and extremes since 1500,
1107 *Science*, 303, 1499–1503, doi:10.1126/science.1093877, 2004.
- 1108 Malanotte-Rizzoli, P., Artale, V., Borzelli-Eusebi, G. L., Brenner, S., Crise, A., Gacic,
1109 M., Kress, N., Marullo, S., Ribera d’Alcalà, M., Sofianos, S., Tanhua, T.,
1110 Theocharis, A., Alvarez, M., Ashkenazy, Y., Bergamasco, A., Cardin, V., Carniel,
1111 S., Civitarese, G., D’Ortenzio, F., Font, J., Garcia-Ladona, E., Garcia-Lafuente, J.
1112 M., Gogou, A., Gregoire, M., Hainbucher, D., Kontoyannis, H., Kovacevic, V.,
1113 Kraskapoulou, E., Kroskos, G., Incarbona, A., Mazzocchi, M. G., Orlic, M., Ozsoy,
1114 E., Pascual, A., Poulain, P.-M., Roether, W., Rubino, A., Schroeder, K., Siokou-
1115 Frangou, J., Souvermezoglou, E., Sprovieri, M., Tintoré, J., and Triantafyllou, G.:
1116 Physical forcing and physical/biochemical variability of the Mediterranean Sea: a
1117 review of unresolved issues and directions for future research, *Ocean Sci.*, 10, 281–
1118 322, doi:10.5194/os-10-281-2014, 2014.
- 1119 Maldonado, A., Got, H., Monaco, A., O’Connell, S., and Mirabile, L.: Valencia Fan
1120 (northwestern Mediterranean): distal deposition fan variant, *Mar. Geol.*, 62, 295–
1121 319, 1985.
- 1122 Mangini, A., Spötl, C., and Verdes, P.: Reconstruction of temperature in the Central
1123 Alps during the past 2000 yr from a $\delta^{18}\text{O}$ stalagmite record, *Earth. Planet. Sci. Lett.*,
1124 235, 741–751, 2005.
- 1125 Mann, M. E., Zhang, Z., Hughes, M. K., Bradley, R. S., Miller, S. K., Rutherford, S.,
1126 and Ni, F.: Proxy-based reconstructions of hemispheric and global surface
1127 temperature variations over the past two millennia, *P. Natl. Acad. Sci. USA*, 105,
1128 13252–13257, 2008.
- 1129 Mann, M. E., Zhang, Z., Rutherford, S., Bradley, R. S., Hughes, M. K., Shindell, D.,
1130 Ammann, C., Faluvegi, G., and Ni, F.: Global signatures and dynamical origins of
1131 the little ice age and medieval climate anomaly, *Science*, 326, 1256–1260, 2009.
- 1132 Marchal, O., Cacho, I., Stocker, T. F., Grimalt, J. O., Calvo, E., Martrat, B., Shackleton,
1133 N., Vautravers, M., Cortijo, E., Van Kreveld, S., Andersson, C., Ko, N., Chapman,
1134 M., Saffi, L., Duplessy, J., Sarnthein, M., and Turon, J.: Apparent long-term
1135 cooling of the sea surface in the northeast Atlantic and Mediterranean during the
1136 Holocene, *Quaternary Sci. Rev.*, 21, 455–483, 2002.
- 1137 Margaritelli G., Lirer F., Vallefucoco M., Bonomo S., Cascella A., Capotondi L., Ferraro
1138 L., Insinga D.D., Petrosino P., Rettori R.: Climatic variability during the last two
1139 millennia in the Tyrrhenian Sea: evidences from planktonic foraminifera and
1140 geochemical data, XV Edizione delle “Giornate di Paleontologia”
1141 PALEODAYS2015, Palermo 17-29 Maggio 2015, 72-73. Società Paleontologica
1142 Italiana, 2015.
- 1143 Mariotti, A.: Decadal climate variability and change in the Mediterranean Region, *Sci.*
1144 *Technol. Infus. Clim. Bull.*, Climate Test Bed Joint Seminar Series, Maryland, US
1145 National Oceanic and Atmospheric Administration, 1–5, 2011.
- 1146 Martin, J., Elbaz-Poulichet, F., Guieu, C., Lo, e-Pilot, M., and Han, G.: River versus

- 1147 atmospheric input of material to the Mediterranean Sea: an Overview, *Mar. Chem.*,
1148 28, 159–182, 1989.
- 1149 Martín-Chivelet, J., Muñoz-García, M. B., Edwards, R. L., Turrero, M. J., and Ortega,
1150 A. I.: Land surface temperature changes in Northern Iberia since 4000 yr BP, based
1151 on $\delta^{13}\text{C}$ of speleothems, *Glob. Planet. Change.*, 77, 1–12,
1152 doi:10.1016/j.gloplacha.2011.02.002, 2011.
- 1153 Martín-Puertas, C., Valero-Garcés, B. L., Brauer, A., Mata, M. P., Delgado-Huertas, A.,
1154 and Dulski, P.: The Iberian–Roman Humid Period (2600–1600 cal yr BP) in the
1155 Zoñar Lake varve record (Andalucía, Southern Spain), *Quaternary Res.*, 71, 2,
1156 doi:10.1016/j.yqres.2008.10.004, 2008.
- 1157 Martínez-Cortizas, A., Pontevedra-Pombal, X., García-Rodeja, E., Nóvoa-Muñoz, J. C.,
1158 and Shotyk, W.: Mercury in a Spanish Peat Bog: archive of climate change and
1159 atmospheric metal deposition, *Science*, 284, 939–942, 1999.
- 1160 Martrat, B., Grimalt, J. O., Lopez-Martinez, C., Cacho, I., Sierro, F. J., Flores, J. A.,
1161 Zahn, R., Canals, M., Curtis, J. H., and Hodell, D. A.: Abrupt temperature changes
1162 in the Western Mediterranean over the past 250 000 years, *Science*, 306, 1762,
1163 doi:10.1126/science.1101706, 2004.
- 1164 Marullo, S., Artale, V., and Santoleri, R.: The SST multi-decadal variability in the
1165 Atlantic-Mediterranean region and its relation to AMO, *J. Climate*, 24, 4385–4401,
1166 doi:10.1175/2011JCLI3884.1, 2011.
- 1167 Mashiotta, T. A., Lea, D. W., and Spero, H. J.: Glacial–interglacial changes in
1168 Subantarctic sea surface temperature and $\delta^{18}\text{O}$ -water using foraminiferal Mg, *Earth*
1169 *Planet. Sc. Lett.*, 170, 417–432, 1999.
- 1170 Masqué, P., Fabres, J., Canals, M., Sanchez-Cabeza, J. A., Sanchez-Vidal, A., Cacho, I.,
1171 Calafat, A. M., and Bruach, J. M.: Accumulation rates of major constituents of
1172 hemipelagic sediments in the deep Alboran Sea: a centennial perspective of
1173 sedimentary dynamics, *Mar. Geol.*, 193, 207–233, 2003.
- 1174 Matthews, J. A. and Bri_a, K. R.: The “Little ice age”: re-evaluation of an evolving
1175 concept, *Geogr. Ann. A*, 87, 17–36, 2005.
- 1176 Mauffret, A.: Etude géodynamique de la marge des Illes Baléares, *Mémoires de la*
1177 *Société Géologique de France LVI*, 1–96, 1979.
- 1178 Mayewski, P. A., Rohling, E. E., Stager, J. C., Karlen, W., Maasch, K. A., Meeker, L.
1179 D., Meyerson, E. A., Gasse, F., van Kreveld, S., Holmgren, K., Lee-Thorp, J.,
1180 Rosqvist, G. Rack, F., Staubwasser, M., Schneider, R. R., and Steig, E. J.: Holocene
1181 climate variability, *Quaternary Res.*, 62, 243–255, 2004.
- 1182 McConnell, M. C. and Thunell, R. C.: Calibration of the planktonic foraminiferal
1183 Mg/Ca paleothermometer: sediment trap results from the Guaymas Basin, Gulf of
1184 California, *Paleoceanography*, 20, PA2016, doi:10.1029/2004PA001077, 2005.
- 1185 McGregor, H. V., Evans, M. N., Goosse, H., Leduc, G., Martrat, B., Addison, J. A.,
1186 Graham Mortyn, P., Oppo, D. W., Seidenkrantz, M.-S., Sicre, M.-A., Phipps, S. J.,
1187 Selvaraj, K., Thirumalai, K., Filipsson, H. L. and Ersek, V.: Robust global ocean
1188 cooling trend for the pre-industrial Common Era, *Nat Geosci*, 8(9), 671–677,
1189 doi:10.1038/ngeo2510, 2015.
- 1190 MEDAR GROUP, MEDATLAS/2002 European Project: Mediterranean and Black Sea
1191 Database of Temperature Salinity and Bio-Chemical Parameters, *Climatological*
1192 *Atlas*, Institut Français de Recherche pour L’Exploitation de la Mer (IFREMER),
1193 Edition/Instituto Nazionale di Oceanografia e di Geofisica Sperimentale (OGS),
1194 2002.
- 1195 Medoc, G.: Observation of formation of Deep Water in the Mediterranean Sea, *Nature*,
1196 227, 1037–1040, 1970.

- 1197 Millán, M. M., Estrela, M. J., Sanz, M. J., Mantilla, E., Martín, M., Pastor, F., Salvador,
1198 R., Vallejo, R., Alonso, L., Gangoiti, G., Iardía, J. L., Navazo, M., Albizuri, A.,
1199 Artiñano, B., Ciccioioli, P., Kallos, G., Carvalho, R. A., Andrés, D., Ho_, A.,
1200 Werhahn, J., Seufert, G., and Versino, B.: Climatic feedbacks and desertification:
1201 the Mediterranean Model, *J. Climate*, 18, 684–701, 2005.
- 1202 Millot, C.: Circulation in the Western Mediterranean Sea, *J. Marine Syst.*, 20, 423–442,
1203 1999.
- 1204 Morellón, M., Pérez-Sanz, A., Corella, J. P., Büntgen, U., Catalán, J., González-
1205 Sampérez, P., González-Trueba, J. J., López-Sáez, J. A., Moreno, A., Pla-Rabes, S.,
1206 Saz-Sánchez, M. Á., Scussolini, P., Serrano, E., Steinhilber, F., Stefanova, V.,
1207 Vegas-Vilarrúbia, T., and Valero-Garcés, B.: A multi-proxy perspective on
1208 millennium-long climate variability in the Southern Pyrenees, *Clim. Past*, 8, 683–
1209 700, doi:10.5194/cp-8-683-2012, 2012.
- 1210 Moreno, A., Cacho, I., Canals, M., Prins, M. A., Sánchez-Goñi, M. F., Grimalt, J. O.,
1211 and Weltje, G. J.: Saharan Dust Transport and High-Latitude Glacial Climatic
1212 Variability: the Alboran Sea Record, *Quaternary Res.*, 58, 318–328,
1213 doi:10.1006/qres.2002.2383, 2002.
- 1214 Moreno, A., Cacho, I., Canals, M., Grimalt, J. O., Sánchez-Goñi, M. F., Shackleton, N.,
1215 and Sierro, F. J.: Links between marine and atmospheric processes oscillating on a
1216 millennial time-scale. A multi-proxy study of the last 50,000 yr from the Alboran
1217 Sea (Western Mediterranean Sea), *Quaternary Sci. Rev.*, 24, 1623–1636,
1218 doi:10.1016/j.quascirev.2004.06.018, 2005.
- 1219 Moreno, A., Valero-Garcés, B. L., González-Sampérez, P., and Rico, M.: Flood
1220 response to rainfall variability during the last 2000 years inferred from the Taravilla
1221 Lake record (Central Iberian Range, Spain), *J. Paleolimnol.*, 40, 943–961,
1222 doi:10.1007/s10933-008-9209-3, 2008.
- 1223 Moreno, A., Pérez, A., Frigola, J., Nieto-Moreno, V., Rodrigo-Gámiz, M., Martrat, B.,
1224 González-Sampérez, P., Morellón, M., Martín-Puertas, C., Pablo, J., Belmonte, Á.,
1225 Sancho, C., Cacho, I., Herrera, G., Canals, M., Grimalt, J. O., Jiménez-Espejo, F.,
1226 Martínez-Ruiz, F., Vegas-Vilarrúbia, T., and Valero-Garcés, B. L.: The Medieval
1227 Climate Anomaly in the Iberian Peninsula reconstructed from marine and lake
1228 records, *Quaternary Sci. Rev.*, 43, 16–32, doi:10.1016/j.quascirev.2012.04.007,
1229 2012.
- 1230 Morhange, C., Marriner, N., Excoffon, P., Bonnet, S., Flaux, C., Zibrowius, H., Goiran,
1231 J. P., and El Amouri, M.: Relative Sea-Level Changes During Roman Times in the
1232 Northwest Mediterranean: the 1st Century AD. Fish Tank of Forum Julii, Fréjus,
1233 France, *Geoarchaeology*, 28, 363–372, doi:10.1002/gea.21444, 2013.
- 1234 Mulitza, S., Boltovskoy, D., Donner, B., Meggers, H., Paul, A. and Wefer, G.:
1235 Temperature: δ 18O relationships of planktonic foraminifera collected from surface
1236 waters, *Palaeogeogr Palaeoclimatol Palaeoecol*, 202(1-2), 143–152,
1237 doi:10.1016/S0031-0182(03)00633-3, 2003.
- 1238 Nieto-Moreno, V., Martínez-Ruiz, F., Giral, S., Jiménez-Espejo, F., Gallego-Torres,
1239 D., Rodrigo-Gámiz, M., García-Orellana, J., Ortega-Huertas, M., and de Lange, G.
1240 J.: Tracking climate variability in the western Mediterranean during the Late
1241 Holocene: a multiproxy approach, *Clim. Past*, 7, 1395–1414, doi:10.5194/cp-7-
1242 1395-2011, 2011.
- 1243 Nieto-Moreno, V., Martínez-Ruiz, F., Willmott, V., García-Orellana, J., and Masqué,
1244 P.: Organic geochemistry climate conditions in the westernmost Mediterranean over
1245 the last two millennia: an integrated biomarker approach, *Org. Geochem.*, 55, 1–10,
1246 doi:10.1016/j.orggeochem.2012.11.001, 2013.

- 1247 Olsen, J., Anderson, N. J., and Knudsen, M. F.: Variability of the North Atlantic
1248 Oscillation over the past 5200 years, *Nat. Geosci.*, 5, 808–812,
1249 doi:10.1038/ngeo1589, 2012.
- 1250 Ortega, P., Lehner, F., Swingedouw, D., Masson-Delmotte, V., Raible, C. C., Casado,
1251 M., and Yiou, P.: A model-tested North Atlantic Oscillation reconstruction for the
1252 past millennium, *Nature*, 523, 7558, doi:10.1038/nature14518, 2015.
- 1253 PAGES: Science Plan and Implementation Strategy, IGBP Report No. 57, IGBP
1254 Secretariat, Stockholm, 2009.
- 1255 PAGES 2K Consortium: Continental-scale temperature variability during the past two
1256 millennia, *Nature*, 6, 339–346, doi:10.1038/NGEO1797, 2013.
- 1257 Pastor, F.: Ciclogénesis intensas en la cuenca occidental del Mediterráneo y temperatura
1258 superficial del mar: modelización y evaluación de las áreas de recarga, PhD Thesis,
1259 Dept. of Astronomy and Meteorology, University of Barcelona, Spain, 2012.
- 1260 Pastor, F., Estrela, M., Peñarrocha, D., and Millán, M.: Torrential rains on the Spanish
1261 Mediterranean Coast: modeling the effects of the sea surface temperature, *J. Appl.*
1262 *Meteorol.*, 40, 1180–1195, 2001.
- 1263 Patton, G. M., Martin, P. A., Voelker, A., and Salgueiro, E.: Multiproxy comparison of
1264 oceanographic temperature during Heinrich Events in the eastern subtropical
1265 Atlantic, *Earth Planet. Sc. Lett.*, 310, 45–58, doi:10.1016/j.epsl.2011.07.028, 2011.
- 1266 Pena, L. D., Calvo, E., Cacho, I., Eggins, S., and Pelejero, C.: Identification and
1267 removal of Mn-Mg-rich contaminant phases on foraminiferal tests: implications for
1268 Mg/Ca past temperature reconstructions, *Geochem. Geophys. Geosy.*, 6, 9,
1269 doi:10.1029/2005GC000930, 2005.
- 1270 Pena, L. D., Cacho, I., Calvo, E., Pelejero, C., Eggins, S., and Sadekov, A.:
1271 Characterization of contaminant phases in foraminifera carbonates by electron
1272 microprobe mapping, *Geochem. Geophys. Geosy.*, 9, 7, doi:10.1029/2008GC002018,
1273 2008.
- 1274 Pierre, C.: The oxygen and carbon isotope distribution in the Mediterranean water
1275 masses, *Mar. Geol.*, 153, 41–55, 1999.
- 1276 Pinardi, N. and Masetti, E.: Variability of the large general circulation of the
1277 Mediterranean Sea from observations and modelling: a review, *Palaeogeogr.*
1278 *Palaeoclimatol.*, 158, 153–173, 2000.
- 1279 Pinot, J. M., López-Jurado, J., and Riera, M.: The CANALES experiment (1996–1998).
1280 Interannual, seasonal, and mesoscale variability of the circulation in the Balearic
1281 Channels, *Prog. Oceanogr.*, 55, 335–370, 2002.
- 1282 Piva, A., Asioli, A., Trincardi, F., Schneider, R. R., and Vigliotti, L.: Late-Holocene
1283 climate variability in the Adriatic Sea (Central Mediterranean), *The Holocene*, 18,
1284 153–167, 2008.
- 1285 Pla, S. and Catalan, J.: Chrysophyte cysts from lake sediments reveal the submillennial
1286 winter/spring climate variability in the northwestern Mediterranean region
1287 throughout the Holocene, *Clim. Dynam.*, 24, 263–278, 2005.
- 1288 Pujol, C. and Vergnaud-Grazzini, C.: Distribution patterns of live planktic foraminifers
1289 as related to regional hydrography and productive systems of the Mediterranean Sea,
1290 *Mar. Micropaleontol.*, 25, 187–217, 1995.
- 1291 Reguera, M. I.: Respuesta del Mediterráneo Occidental a los cambios climáticos
1292 bruscos ocurridos durante el último glacial: estudio de las asociaciones de
1293 foraminíferos, PhD Thesis, Dept. of Geology, University of Salamanca, Spain, 2004.
- 1294 Reimer, P. J., Bard, E., Bayliss, A., Beck, J. W., Blackwell, P. G., Bronk Ramsey, C.,
1295 Buck, C. E., Edwards, R. L., Friedrich, M., Grootes, P. M., Guilderson, T. P.,
1296 Haflidason, H., Hajdas, I., Hatté, C., Heaton, T. J., Ho_mann, D. L., Hogg, A. G.,

- 1297 Hughen, K. A., Kaiser, K. F., Kromer, B., Manning, S. W., Niu, M., Reimer, R. W.,
 1298 Richards, D. A., Scott, M. E., Southon, J. R., Turney, C. S. M., and van der Plicht,
 1299 J.: Intcal13 and Marine13 radiocarbon age calibration curves 0–50 000 years cal BP,
 1300 Radiocarbon, 55, 1869–1887, 2013.
- 1301 Richter, T. O. and van der Gaast, S.: The Avaatech Core Scanner: technical description
 1302 and applications to NE Atlantic sediments, in: New Ways of Looking at Sediment
 1303 Core and Core Data, edited by: Rothwell, R. G., Geological Society Special
 1304 Publication, London, 39–50, 2006.
- 1305 Rigual-Hernández, A. S., Sierro, F. J., Bárcena, M. A., Flores, J. A., and Heussner, S.:
 1306 Seasonal and interannual changes of planktic foraminiferal fluxes in the Gulf of
 1307 Lions (NW Mediterranean) and their implications for paleoceanographic studies:
 1308 two 12-year sediment trap records, Deep-Sea Res. Pt. I, 66, 26–40,
 1309 doi:10.1016/j.dsr.2012.03.011, 2012.
- 1310 Rigual-Hernández, A. S., Bárcena, M. A., Jordan, R. W., Sierro, F. J., Flores, J. A.,
 1311 Meier, K. J., Beaufort, L., and Heussner, S.: Diatom fluxes in the NW
 1312 Mediterranean: evidence from a 12-year sediment trap record and surficial
 1313 sediments, J. Plankton. Res., 35, 5, doi:10.1093/plankt/fbt055, 2013.
- 1314 Roberts, N., Moreno, A., Valero-Garcés, B. L., Corella, J. P., Jones, M., Allcock, S.,
 1315 Woodbridge, J., Morellón, M., Luterbacher, J., Xoplaki, E., and Türkeş, M.:
 1316 Palaeolimnological evidence for an east–west climate see-saw in the Mediterranean
 1317 since AD 900, Global Planet. Change, 84–85, 23–34,
 1318 doi:10.1016/j.gloplacha.2011.11.002, 2012.
- 1319 Rodrigo-Gámiz, M., Martínez-Ruiz, S., Rampen, S., Schouten, S., and Sinninghe
 1320 Damsté, J.: Sea surface temperature variations in the western Mediterranean Sea
 1321 over the last 20 kyr: a dual-organic proxy (U^{k}_{37} and LDI) approach,
 1322 Paleoceanography, 29, 87–98, doi:10.1002/2013PA002466, 2014.
- 1323 Rogerson, M., Rohling, E. J., Weaver, P. P. E., and Murray, J. W.: The Azores Front
 1324 since the Last Glacial Maximum, Earth Planet. Sc. Lett., 222, 779–789,
 1325 doi:10.1016/j.epsl.2004.03.039, 2004.
- 1326 Rohling, E., Hayes, A., De Rijk, S., Kroon, D., Zachariasse, W. J., and Eisma, D.:
 1327 Abrupt cold spells in the northwest Mediterranean, Paleoceanography, 13, 316–322,
 1328 1998.
- 1329 Sabatier, P., Dezileau, L., Colin, C., Briquieu, L., Bouchette, F., Martinez, P., Siani, G.,
 1330 Raynal, O., and Von Grafenstein, U.: 7000 years of paleostorm activity in the NW
 1331 Mediterranean Sea in response to Holocene climate events, Quaternary Res., 77, 1–
 1332 11, doi:10.1016/j.yqres.2011.09.002, 2012.
- 1333 Sáez de Cámara, E., Gangoiti, G., Alonso, L., and Iza, J.: Daily precipitation in
 1334 Northern Iberia: understanding the recent changes after the circulation variability in
 1335 the North Atlantic sector, J. Geophys. Res., 120, 19, doi:10.1002/2015JD023306,
 1336 2015.
- 1337 Sanchez-Cabeza, J., Masqué, P., and Ani-Ragolta, I.: ^{210}Pb and ^{210}Po analysis in
 1338 sediments and soils by microwave acid digestion, J. Radioanal. Nucl. Ch., 227, 19–
 1339 22, 1998.
- 1340 Schiebel, R., Schmuker, B., Alves, M., and Hemleben, C.: Tracking the Recent and Late
 1341 Pleistocene Azores front by the distribution of planktic foraminifers, J. Marine Syst.,
 1342 37, 213–227, 2002.
- 1343 Schilman, B., Bar-Matthews, M., Almogilabin, A., and Luz, B.: Global climate
 1344 instability reflected by Eastern Mediterranean marine records during the late
 1345 Holocene, Palaeogeogr. Palaeocl., 176, 157–176, 2001.
- 1346 Shackleton, N.: Attainment of isotopic equilibrium between ocean water and the

1347 benthonic foraminifera genus *Uvigerina*: isotopic changes in the ocean during the
1348 last glacial, CNRS, Colloq. Int., 219, 203–209, 1974.

1349 Sicre, A., Ternois, Y., Miquel, J. C., and Marty, J. C.: Alkenones in the Northwestern
1350 Mediterranean sea: interannual variability and vertical transfer, *Geophys. Res. Lett.*,
1351 26, 1735–1738, 1999.

1352 Sicre, M. A., Yiou, P., Eiríksson, J., Ezat, U., Guimbaut, E., Dahhaoui, I., Knudsen, K.
1353 L., Jansen, E., and Turon, J. L.: A 4500-year reconstruction of sea surface
1354 temperature variability at decadal time-scales off North Iceland, *Quaternary Sci.*
1355 *Rev.*, 27, 2041–2047, doi:10.1016/j.quascirev.2008.08.009, 2008.

1356 Sierra, F. J., Hodell, D. A., Curtis, J. H., Flores, J. A., Reguera, I., Colmenero-Hidalgo,
1357 E., Bárcena, M. A., Grimalt, J. O., Cacho, I., Frigola, J., and Canals, M.: Impact of
1358 iceberg melting on Mediterranean thermohaline circulation during Heinrich events,
1359 *Paleoceanography*, 20, 1–13, doi:10.1029/2004PA001051, 2005.

1360 Siokou-Frangou, I., Christaki, U., Mazzocchi, M. G., Montresor, M., Ribera d’Alcalá,
1361 M., Vaqué, D., and Zingone, A.: Plankton in the open Mediterranean Sea: a review,
1362 *Biogeosciences*, 7, 1543–1586, doi:10.5194/bg-7-1543-2010, 2010.

1363 Sprovieri, R., Stefano, E. Di, Incarbona, A., and Gargano, M. E.: A high-resolution
1364 record of the last deglaciation in the Sicily Channel based on foraminifera and
1365 calcareous nannofossil quantitative distribution, *Palaeogeogr. Palaeoclimatol.*, 202, 119–
1366 142, doi:10.1016/S0031-0182(03)00632-1, 2003.

1367 Steinhilber, F., Beer, J., and Fröhlich, C.: Total solar irradiance during the Holocene,
1368 *Geophys. Res. Lett.*, 36, L19704, doi:10.1029/2009GL040142, 2009.

1369 Steinhilber, F., Abreu, J. A., Beer, J., Brunner, I., Christl, M., Fischer, H., Heikkilä, U.,
1370 Kubik, P. W., Mann, M., McCracken, K. G., Miller, H., Miyahara, H., Oerter, H.,
1371 and Wilhelms, F.: 9400 years of cosmic radiation and solar activity from ice cores
1372 and tree rings, *P. Natl. Acad. Sci. USA*, 109, 5967–5971,
1373 doi:10.1073/pnas.1118965109, 2012.

1374 Stine, S.: Extreme and persistent drought in California and Patagonia during medieval
1375 time, *Nature*, 369, 546–549, 1994.

1376 Stothers, R. B.: Mystery cloud of AD 536, *Nature*, 307, 344–345,
1377 doi:10.1038/307344a0, 1984.

1378 Stuiver, M. and Reimer, P. J.: Extended ¹⁴C data base and revised Calib 3.0 ¹⁴C age
1379 calibration program, *Radiocarbon*, 35, 215–230, 1993.

1380 Taricco, C., Ghil, M., Alessio, S., and Vivaldo, G.: Two millennia of climate variability
1381 in the Central Mediterranean, *Clim. Past*, 5, 171–181, doi:10.5194/cp-5-171-2009,
1382 2009.

1383 Taricco, C., Vivaldo, G., Alessio, S., Rubinetti, S., and Mancuso, S.: A high-resolution
1384 $\delta^{18}\text{O}$ record and Mediterranean climate variability, *Clim. Past*, 11, 509–522,
1385 doi:10.5194/cp-11-509-2015, 2015.

1386 Ternois, Y., Sicre, M. A., Boireau, A., Marty, J. C., Miquel, J. C.: Production pattern of
1387 alkenones in the Mediterranean Sea, *Geophys. Res. Lett.*, 23, 3171–3174, 1996.

1388 Thornalley, D. J. R., Elderfield, H., and McCave, I. N.: Holocene oscillations in
1389 temperature and salinity of the surface subpolar North Atlantic., *Nature*, 457, 711–
1390 714, doi:10.1038/nature07717, 2009.

1391 Thunell, R.C.: Distribution of Recent Planktonic Foraminifera in Surface Sediments of
1392 the Mediterranean Sea, *Mar Micropaleontol.*, 3, 147–173, 1978.

1393 Touchan, R., Xoplaki, E., Funkhouser, G., Luterbacher, J., Hughes, M. K., Erkan, N.,
1394 Akkemik, Ü., and Stephan, J.: Reconstructions of spring/summer precipitation for
1395 the Eastern Mediterranean from tree-ring widths and its connection to large-scale
1396 atmospheric circulation, *Clim. Dynam.*, 25, 75–98, 2005.

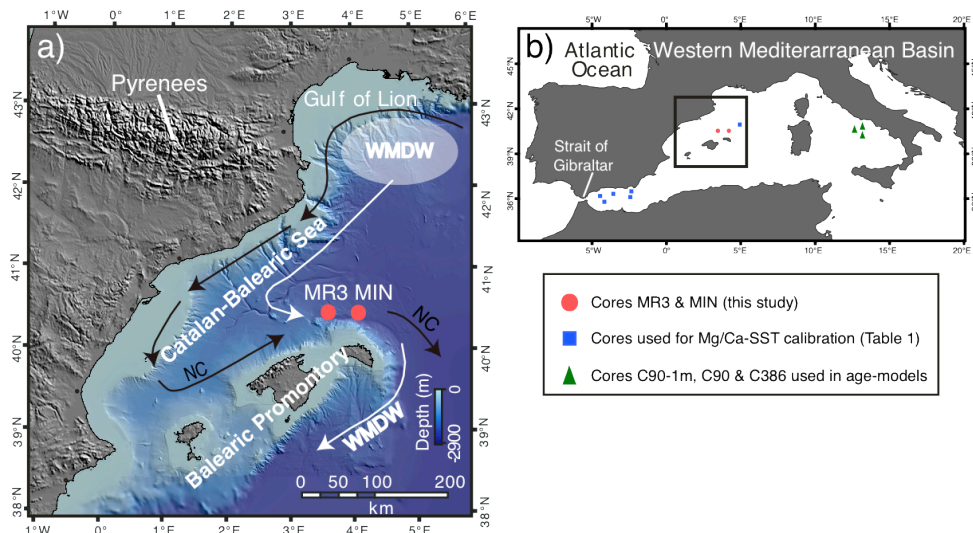
- 1397 Touchan, R., Akkemik, Ü., Hughes, M. K., Erkan, N.: May–June precipitation
 1398 reconstruction of southwestern Anatolia, Turkey during the last 900 years from tree
 1399 rings, *Quaternary Res.*, 68, 196–202, 2007.
- 1400 Trouet, V., Esper, J., Graham, N. E., Baker, A., Scourse, J. D., and Frank, D. C.:
 1401 Persistent positive North Atlantic Oscillation mode dominated the Medieval Climate
 1402 Anomaly, *Science*, 324, 78, doi:10.1126/science.1166349, 2009.
- 1403 Trouet, V., Scourse, J. D., and Raible, C. C.: North Atlantic storminess and Atlantic
 1404 Meridional Overturning Circulation during the last Millennium: reconciling
 1405 contradictory proxy records of NAO variability, *Global Planet. Change*, 84–85, 48–
 1406 55, doi:10.1016/j.gloplacha.2011.10.003, 2012.
- 1407 Tsimplis, M. N. and Baker, F.: Sea level drop in the Mediterranean Sea: an indicator of
 1408 deep water salinity and temperature changes?, *Geophys. Res. Lett.*, 27, 1731–1734,
 1409 2000.
- 1410 Tsimplis, M. N. and Josey, S. A.: Forcing of the Mediterranean Sea by atmospheric
 1411 oscillations over the North Atlantic, *Geophys. Res. Lett.*, 28, 803–806, 2001.
- 1412 Tsimplis, M. N. and Rixen, M.: Sea level in the Mediterranean Sea: the contribution of
 1413 temperature and salinity changes, *Geophys. Res. Lett.*, 29, 1–4,
 1414 doi:10.1029/2002GL015870, 2002.
- 1415 Vallefucio, M., Lirer, F., Ferraro, L., Pelosi, N., Capotondi, L., Sprovieri, M., and
 1416 Incarbona, A.: Climatic variability and anthropogenic signatures in the Gulf of
 1417 Salerno (southern-eastern Tyrrhenian Sea) during the last half millennium, *Rend*
 1418 *Lincei*, 23, 13–23, doi:10.1007/s12210-011-0154-0, 2012.
- 1419 van Raden, U. J., Groeneveld, J., Raitzsch, M., and Kucera, M.: Mg/Ca in the
 1420 planktonic foraminifera *Globorotalia inflata* and *Globigerinoides bulloides* from
 1421 Western Mediterranean plankton tow and core top samples, *Mar. Micropaleontol.*,
 1422 78, 101–112, doi:10.1016/j.marmicro.2010.11.002, 2011.
- 1423 Vargas-Yáñez, M., Moya, F., García-Martínez, M. C., Tel, E., Zunino, P., Plaza, F.,
 1424 Salat, J., and Pascual, J.: Climate change in the Western Mediterranean Sea 1900–
 1425 2008, *J. Marine Syst.*, 82, 171–176, doi:10.1016/j.jmarsys.2010.04.013, 2010.
- 1426 Velasco, J. P. B., Baraza, J., and Canals, M.: La depresión periférica y el lomo
 1427 contourítico de Menorca: evidencias de la actividad de corrientes de fondo al N del
 1428 Talud Balear, *Geogaceta*, 20, 359–362, 1996.
- 1429 Versteegh, G. J. M., de Leeuw, J.W., Taricco, C., and Romero, A.: Temperature and
 1430 productivity influences on $U^{K'}_{37}$ and their possible relation to solar forcing of the
 1431 Mediterranean winter, *Geochem. Geophys. Geosy.*, 8, Q09005,
 1432 doi:10.1029/2006GC001543, 2007.
- 1433 Villanueva, J., Pelejero, C., and Grimalt, J. O.: Clean-up procedures for the unbiased
 1434 estimation of C_{37} alkenone sea surface temperatures and terrigenous n-alkane inputs
 1435 in paleoceanography, *J. Chromatogr.*, 757, 145–151, 1997.
- 1436 Wallace, J. M. and Gutzler, D. S.: Teleconnections in the geopotential height field
 1437 during the Northern Hemisphere winter, *Mon. Weather Rev.*, 109, 784–812, 1981.
- 1438 Wassenburg, J. A., Immenhauser, A., Richter, D. K., Niedermayr, A., and Riechelmann,
 1439 S.: Moroccan speleothem and tree ring records suggest a variable positive state of
 1440 the North Atlantic Oscillation during the Medieval Warm Period, *Earth Planet. Sc.*
 1441 *Lett.*, 375, 291–302, doi:10.1016/j.epsl.2013.05.048, 2013.
- 1442 Weldeab, S., Siebel, W., Wehausen, R., Emeis, K., Schmiedl, G., and Hemleben, C.:
 1443 Late Pleistocene sedimentation in the western Mediterranean Sea: implications for
 1444 productivity changes and climatic conditions in the catchment areas, *Palaeogeogr.*
 1445 *Palaeoclimatol.*, 190, 121–137, 2003.
- 1446 Wright, H. E.: *Global Climates since the Last Glacial Maximum*, Minnesota University

- 1447 Press, Minneapolis, 1994.
- 1448 Yu, J., Elderfield, H., Greaves, M., and Day, J.: Preferential dissolution of benthic
1449 foraminiferal calcite during laboratory reductive cleaning, *Geochem. Geophys.*
1450 *Geosy.*, 8, 6, doi:10.1029/2006GC001571, 2007.
- 1451 Zúñiga, D., García-Orellana, J., Calafat, A., Price, N. B., Adatte, T., Sanchez-Vidal, A.,
1452 Canals, M., Sanchez-Cabeza, J. A., Masqué, P., and Fabres, J.: Late Holocene fine-
1453 grained sediments of the Balearic Abyssal Plain, Western Mediterranean Sea, *Mar.*
1454 *Geol.*, 237, 25–36, 2007.

1455
1456
1457
1458
1459
1460

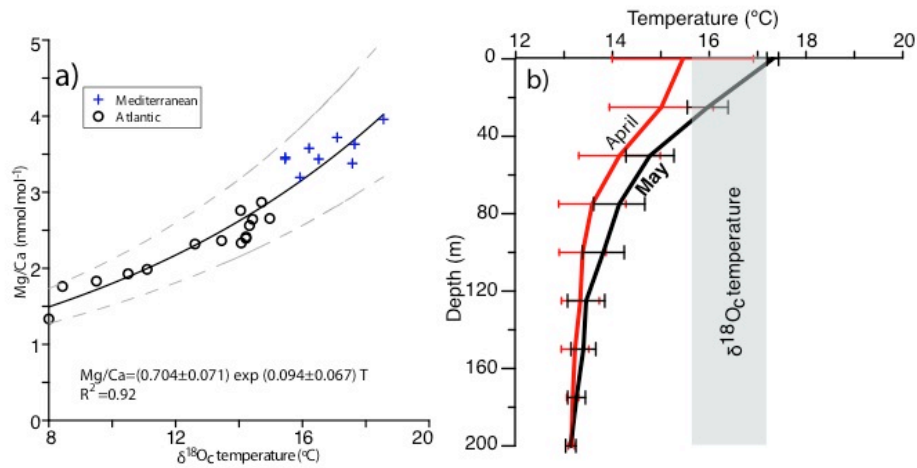
Table 1. Core tops taken into account in the calibration's adjustment. $\delta^{18}\text{O}_c$ and Mg/Ca have been obtained by means of analyses on *G. bulloides* (Mg/Ca procedure have been performed without reductive step).

Core	Location	Latitude	Longitude	Mg/Ca (mmol mol ⁻¹)	$\delta^{18}\text{O}_c$ (VPDB‰)
TR4-157	Balearic Abyssal Plain	40° 30.00' N	4° 55.76' E	3.36	0.53
ALB1	Alboran Sea (WMed)	36° 14.31' N	4° 15.52' W	3.20	0.80
ALBT1	Alboran Sea (WMed)	36° 22.05' N	4° 18.14' W	3.44	0.65
ALBT2	Alboran Sea (EMed)	36° 06.09' N	3° 02.41' W	3.63	0.57
ALBT4	Alboran Sea (EMed)	36° 39.63' N	1° 32.35' W	3.72	0.93
ALBT5	Alboran Sea (EMed)	36° 13.60' N	1° 35.97' W	3.38	0.64



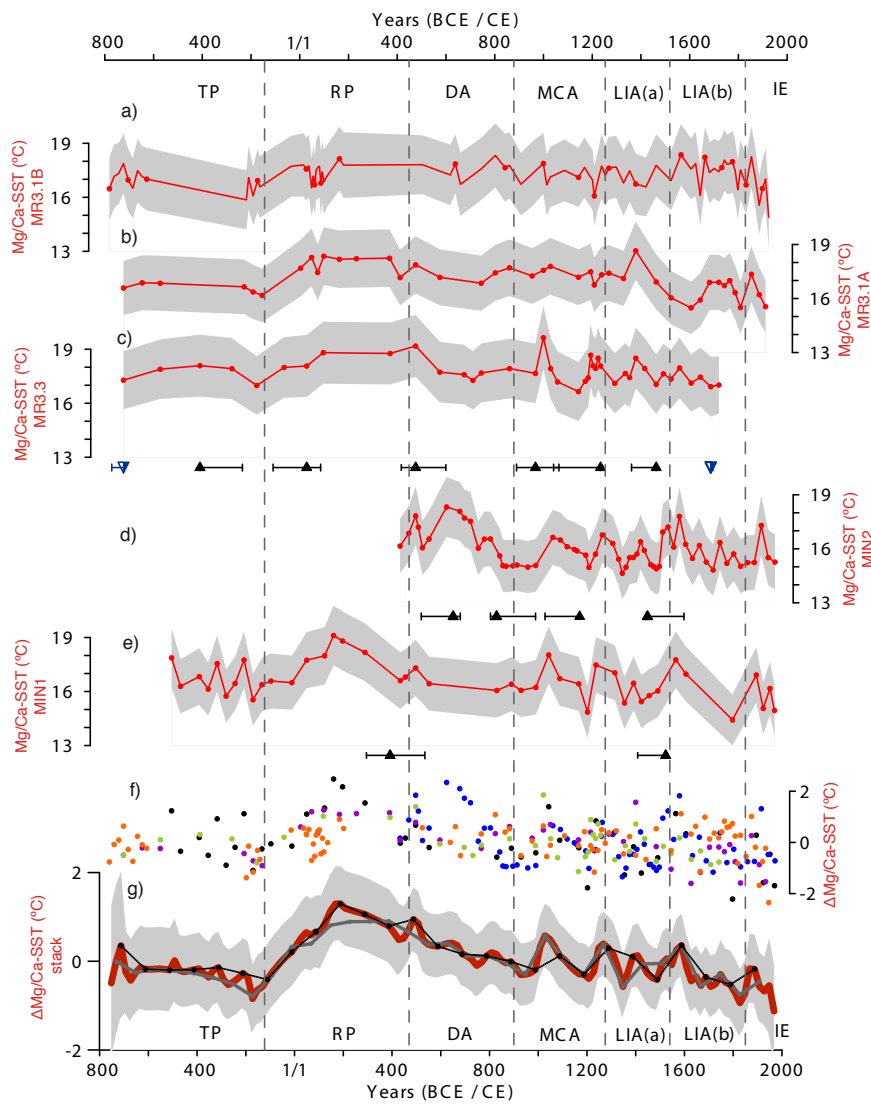
1
2

3 Figure 1. Location of the studied area. (a) Central-western Mediterranean Sea: cores MIN
4 and MR3 effect of this study (red dots) with relevant features of surface (NC: Northern
5 Current) and deep water circulation (WMDW: Western Mediterranean Deep Water). (b)
6 Cores used in age-models development from the Tyrrhenian Sea (green triangles) (Lirer et
7 al., 2013) and cores used in Mg/Ca-SST calibration from the Western Mediterranean
8 Basin (blue squares).



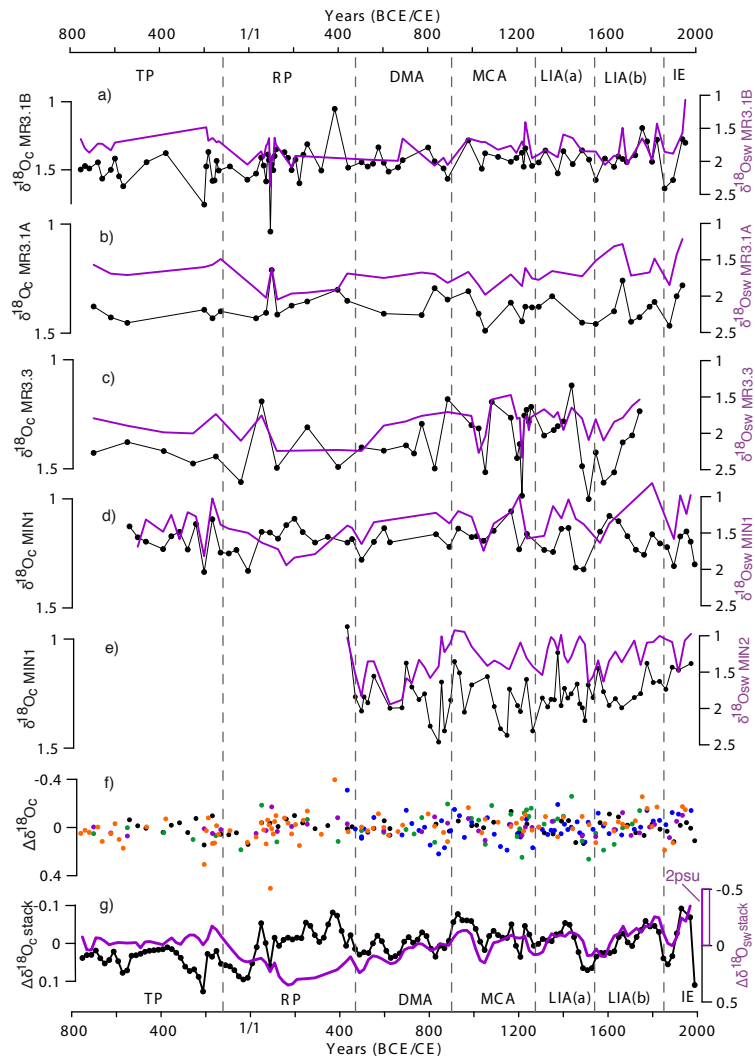
1
2

3 Figure 2. (a) Exponential function and correlation obtained between δ¹⁸O_c temperatures
 4 and Mg/Ca for western Mediterranean Sea. Dashed lines show the 1σ confidence limits of
 5 the curve fit. The standard error of our temperature calibration taking into account each
 6 δ¹⁸O_c -temperatures from core tops (Table 1) is ± 0.6°C. Error of temperature estimates
 7 based on our *G.bulloides* calibration for the Western Mediterranean is ± 1.4°C. These
 8 uncertainties are higher but still in the range than ± 0.6°C obtained for the Atlantic Ocean
 9 in Elderfield and Ganssen (2000) and also 1.1°C in the same sp. culture data (Lea et al.,
 10 1999). (b) April (red) and May (black) temperature profiles of the first 200 m measured
 11 during years 1945-2000 in stations corresponding to the studied core tops (MEDAR
 12 GROUP, 2002). In grey is shown the δ¹⁸O_c average temperature of all cores.



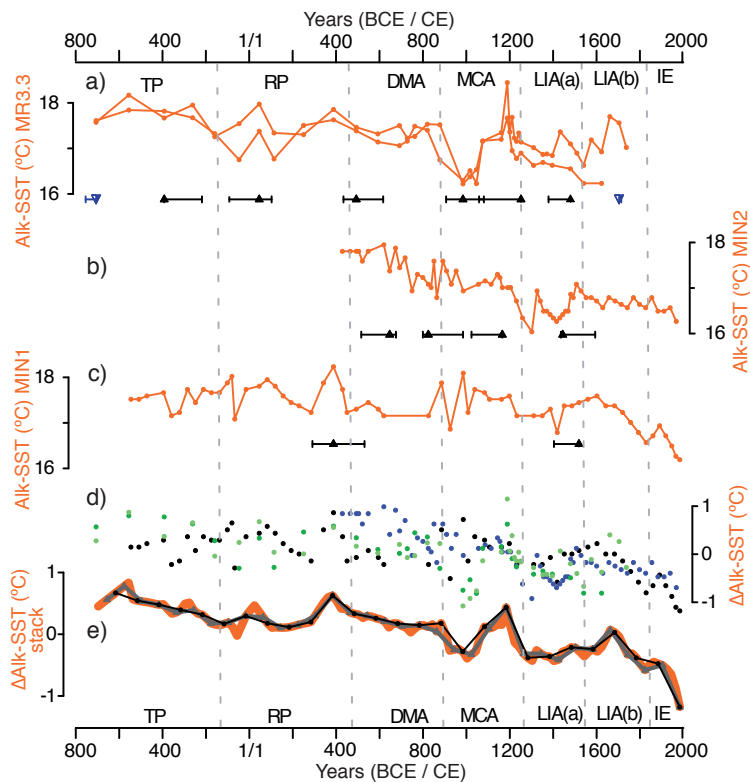
1
2
3
4
5
6
7
8
9
10
11
12
13

Figure 3. SST obtained by means of analysis of Mg/Ca for cores: (a) MR3.1B, (b) MR3.1A, (c) MR3.3, (d) MIN2 and (e) MIN1. Grey-scales integrate uncertainties of average values represent 1σ ; of absolute values include analytical precision and reproducibility and also uncertainties derived *G. bulloides* core top calibrations for the central-western Mediterranean Sea developed in this paper. (f) All individual SST anomalies on their respective time step (MR3.1B: orange, MR3.1A: purple, MR3.3: green, MIN2: blue and MIN1: black dots). (g) 20 yr cm^{-1} stacked temperature anomaly (red plot) with its 2σ uncertainty (grey band). The 80 yr cm^{-1} (grey plot) and the 100 yr cm^{-1} (black plot) stacks are also shown. Triangles represent to ^{14}C dates (black) and biostratigraphical dates based on planktonic foraminifera (blue) and they are shown below the corresponding core and with their associated 2σ errors.



1
2

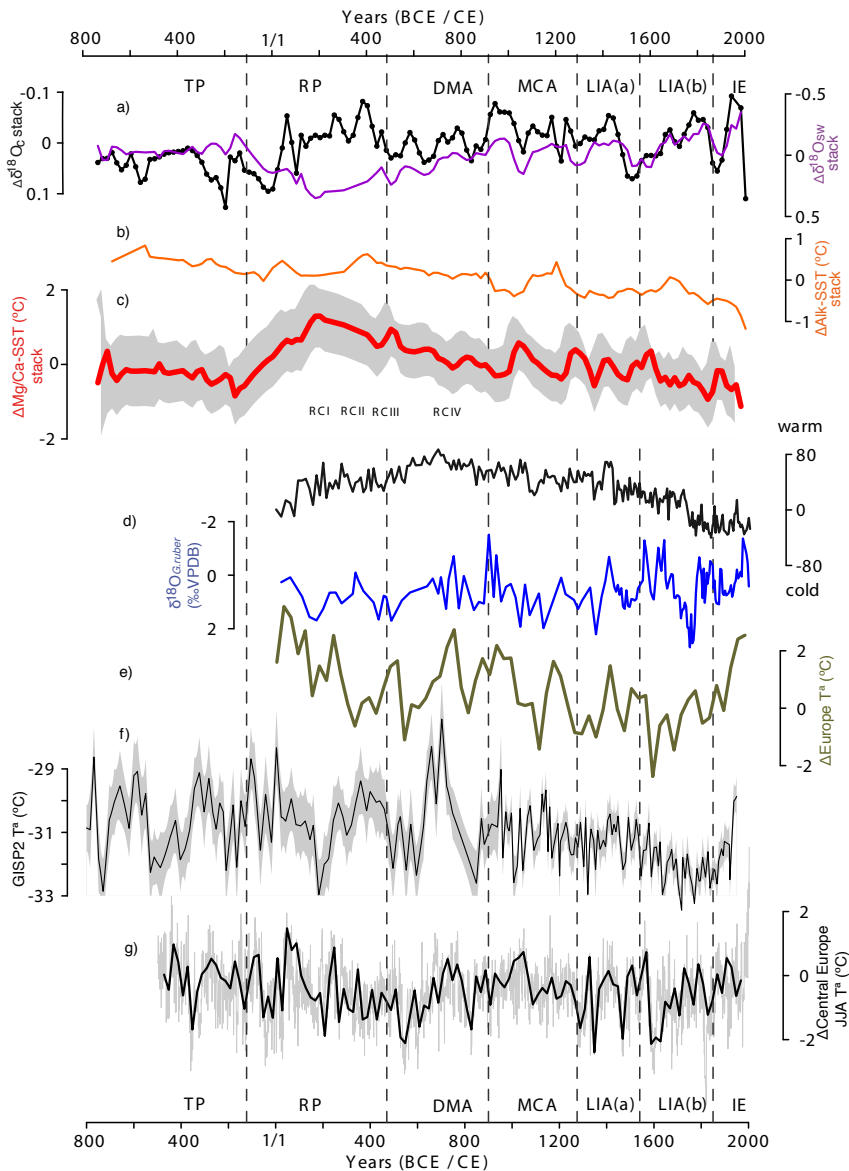
3 Figure 4. Oxygen isotope measured on carbonates shells of *G. bulloides* ($\delta^{18}\text{O}_c$ VPDB‰,
 4 in black) and their derived $\delta^{18}\text{O}_{sw}$ (purple) for cores: (a) MR3.1B, (b) MR3.1A, (c)
 5 MR3.3 (d) MIN2 and (e) MIN1. (f) Individual $\delta^{18}\text{O}_c$ (VPDB‰) anomalies on their
 6 respective time step. (g) Both respective anomaly stacked records and the equivalence
 7 between $\delta^{18}\text{O}_{sw}$ (SMOW‰) and salinity, calculated according to Pierre (1999). It is
 8 estimated that the rise of one unit of $\delta^{18}\text{O}_{sw}$ would amount to an enhancement of 4
 9 practical salinity units.



1

2

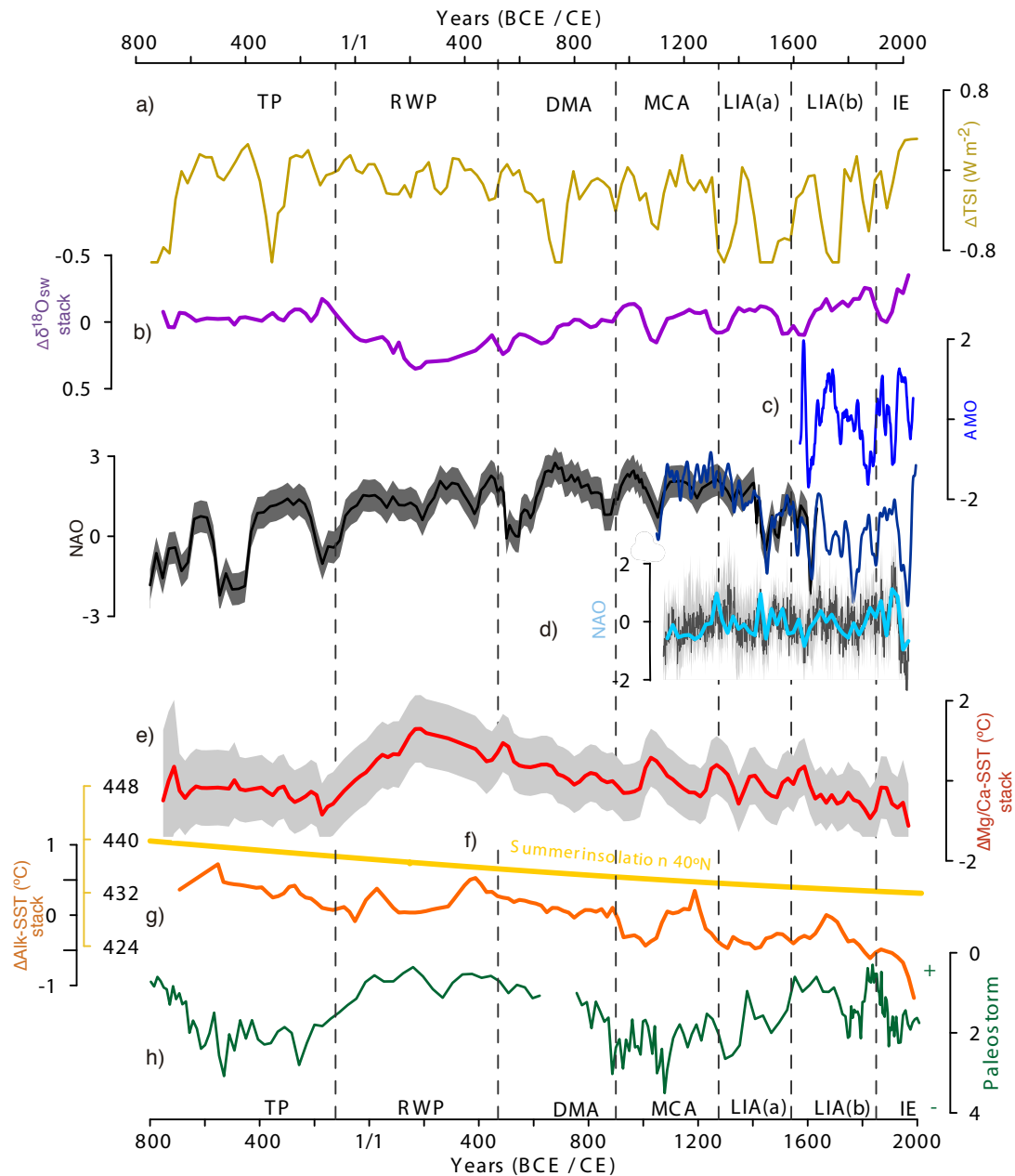
3 Figure 5. Alkenone temperature records from Minorca (this study) for cores: (a) MR3.3,
 4 (b) MIN2 and (c) MIN1. Triangles represent to ^{14}C dates (black) and biostratigraphical
 5 dates based on planktonic foraminifera (blue) and they are shown below the corresponding
 6 core and with their associated 2σ errors. (d) All individual alkenone derived SST
 7 anomalies on their respective time step (MR3.3: green, MIN2: blue and MIN1: black
 8 dots); (e) 20 yr cm^{-1} stacked temperature anomaly (orange plot). The 80 yr cm^{-1} (grey plot)
 9 and the 100 yr cm^{-1} (black plot) stacks are also shown.



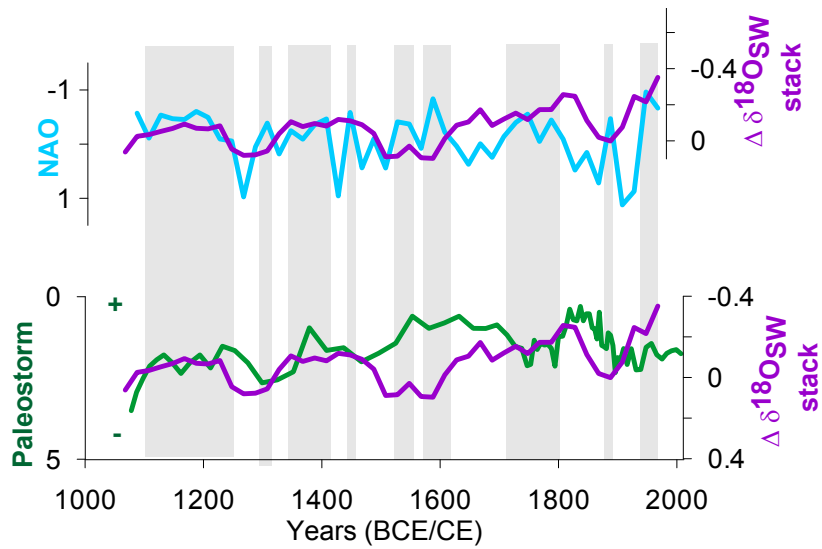
1

2

3 Figure 6. Temperature and isotope anomaly records from Minorca (this study) and data
 4 from other regions. (a) $\delta^{18}\text{O}_c$ (VPDB‰) and $\delta^{18}\text{O}_{\text{SW}}$ (SMOW‰) Minorca stacks, (b)
 5 Alkenone-SST anomaly Minorca stack, (c) Mg/Ca-SST anomaly Minorca stack, (d) warm
 6 and cold phases and $\delta^{18}\text{O}_{\text{G.ruber}}$ recorded by planktonic foraminifera from the southern
 7 Tyrrhenian composite core, respectively and RCI to RCIV showing roman cold periods
 8 (Lirer et al., 2014), (e) 30-year averages of the PAGES 2k Network (2013) Europe
 9 anomaly Temperature reconstruction, (f) Greenland snow surface temperature (Kobashi et
 10 al., 2011) and (g) Central Europe Summer anomaly temperature reconstruction in Central
 11 Europe (Büntgen et al., 2011).



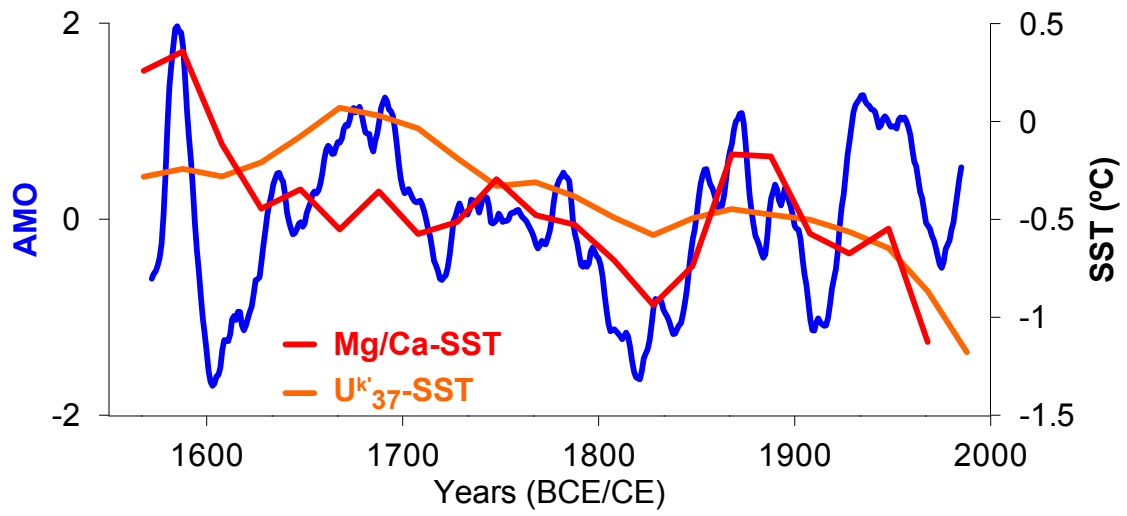
1
 2
 3 Figure 7. Temperature and isotope anomaly records from Minorca (this study) and data
 4 from other regions and with external forcings: (a) Total Solar Irradiance (Steinhilber et
 5 al., 2009, 2012), (b) $\delta^{18}\text{O}_{\text{sw}}$ Minorca stacks, (c) Atlantic Multidecadal Oscillation (AMO)
 6 (Gray et al., 2004), (d) North Atlantic Oscillation (NAO) reconstructions (Olsen et al.,
 7 2012, Trouet et al., 2009, and for the last millennium: Ortega et al., 2015), (e) Mg/Ca-SST
 8 anomaly Minorca stack, (f) Summer Insolation at 40°N (Laskar et al., 2004), (g)
 9 Alkenone-SST anomaly Minorca stack and (h) Paleostorm activity in the Gulf of Lions
 10 (Sabatier et al., 2012).



1

2 Figure 8. $\delta^{18}\text{O}_{\text{sw}}$ Minorca stack (SMOW‰) during the last millennium (age is expressed
 3 in years Common Era) plotted with (a) NAO reconstruction (Ortega et al., 2015) and (b)
 4 Paleostorm activity in the Gulf of Lion (Sabatier et al., 2012). Notice that the NAO axis is
 5 on descending scale. Grey vertical bars represent negative NAO phases.

1



2

3 Figure 9. Mg/Ca-SST and Alkenone-SST Minorca anomaly stacks during the last
4 centuries plotted with AMO reconstruction (Gray et al., 2004).